LA-UR-13-28693
Approved for public release; distribution is unlimited.

Title: Electromagnetic and Beam-Dynamics Modeling of the New LANL RFQ with CST Studio

Author(s): Kurennoy, Sergey S.

Intended for: Distribution to external collaborators

Issued: 2013-11-12

Los Alamos
NATIONAL LABORATORY

Technical Note

Accelerator Operation and Technology
AOT-HPE: High-Power Electrodynamics

To/MS: Distribution
From/MS: Sergey Kurennoy, AOT-HPE / H817
Phone/Fax: 505-665-1459 / 505-665-2904
E-mail: kurennoy@lanl.gov

Symbol: AOT-HPE: 13-008 (TN)
Date: October 30, 2013

SUBJECT: Electromagnetic and Beam-Dynamics Modeling of the New LANL RFQ with CST Studio.

The CST Studio Suite [1] is used to evaluate the design and performance of the new 4-rod LANL proton RFQ. Starting with a detailed engineering CAD model, an electromagnetic analysis of the RFQ is performed with the CST MicroWave Studio (MWS). The MWS-calculated RF fields are used for PIC modeling of beam dynamics in the RFQ with CST Particle Studio (PS) and for thermal-stress analysis with ANSYS. This technical note describes our RFQ modeling and summarizes its results.

Distribution:

AOT-HPE File			(e-mail copy)
AOT-HPE			(e-mail copy)
B.E. Carlsten	AOT-DO	MS H817	(e-mail copy)
R.W. Garnett	AOT-DO	MS H817	(e-mail copy)
J.L. Erickson	AOT-DO	MS H809	(e-mail copy)
S. Nath	AOT-DO	MS H809	(e-mail copy)
M.J. Borden	AOT-MDE	MS H838	(e-mail copy)
J.F. O'Hara	AOT-MDE	MS H838	(e-mail copy)
E.R. Olivas	AOT-MDE	MS H838	(e-mail copy)
W.M. Tuzel	AOT-MDE	MS H838	(e-mail copy)
Y.K. Batygin	AOT-OPS	MS H817	(e-mail copy)
R.C. McCrady	AOT-OPS	MS H817	(e-mail copy)
D.E. Rees	AOT-RFE	MS H827	(e-mail copy)
J.T. Lyles	AOT-RFE	MS H827	(e-mail copy)

1. Introduction.

A new RFQ-based front end is planned for the LANSCE accelerator complex, initially to replace the existing Cockroft-Walton proton injection [2]. A 4-rod type RFQ design was developed in collaboration between IAP (Frankfurt, Germany) and LANL. The new LANL RFQ, operating at 201.25 MHz at the duty factor up to 15%, with 35-keV injection and 750-keV final energy, should satisfy special requirements due to its incorporation into the existing medium-energy beam transfer that works with multiple beams [3]. The RFQ will be manufactured by Kress GmbH. To be prepared to evaluate its design in detail, we have studied a 4-rod RFQ, which was recently designed by the IAP for Fermilab, fabricated by Kress GmbH, and then installed and operated at FNAL [4]. Many parameters of the FNAL RFQ are similar to those for LANSCE: the same RF frequency, 201.25 MHz, and the input and output energies, 35 and 750 keV, respectively. The major difference is the duty factor, which is very low, 0.12%, for the Fermilab design. Our CST modeling of the FNAL RFQ helped our Fermilab colleagues fix some problems, in particular, the low output energy. The results of the FNAL RFQ modeling were summarized in [5]; details of EM analysis and PIC simulations are available in technical notes [6].

We received CAD files of the new LANL RFQ from Kress in April 2013. They were imported into CST Studio [1] to create a model and evaluate its performance. Based on the simulation results, we suggested some design modifications. A modified RFQ design was received at LANL in July 2013. Our CST modeling confirmed that this design satisfies the requirements. The new LANL RFQ is now being fabricated. A short summary of our modeling was presented at NA-PAC [7]; here we document all important details.

A CST model of the LANL RFQ and its electromagnetic (EM) analysis with the MicroWave Studio (MWS) are presented in Sec. 2. The MWS-calculated RF fields are used to simulate the beam propagation through the RFQ using a particle-in-cell (PIC) solver in the CST Particle Studio (PS). The beam dynamics modeling with PS is described in Sec. 3. The fields are also used to calculate the power flux due to RF losses, which serves as a thermal load for an engineering analysis performed with ANSYS by MDE engineers (E. Olivas, J. O'Hara). Some results of the thermal-stress analysis are presented in Sec. 4.

2. MWS model of LANL RFQ and EM analysis.

22 stems. The original RFQ CAD model (April 2013) imported in the MWS is shown in Fig. 1. It includes hundreds of auxiliary details that are unessential for EM analysis, from a support stand to RF and vacuum ports to bolts. From Fig. 1 one can see how the RFQ will be oriented after installation: the RFQ box will be rotated by 45 degrees around the axis in the transverse plane (*y*-*z* plane in Fig. 1). The lid of the RFQ vacuum vessel is hidden in Fig. 1 to show the inner parts: vanes and stems; one can see hinges that allow opening this lid. The four modulated RFQ electrodes (vanes) are supported by 22 stems. The vane modulation profile was calculated in the iterations of the RFQ physics design with PARMTEQM [8] and finalized in February 2013, which fixed the RFQ cavity length along the axis at 175 cm, wall to wall. Two design options were suggested: one with evenly spaced stems (equidistant – option E), and another with a variable period between stems (option V), where the spacing between three last stems near each end, 77 mm, is shorter than in the center, 82 mm. The engineering details irrelevant for EM calculations were removed in simplified MWS models. The MWS model for the option V with variable period is shown in Fig. 2. The RFQ box cavity was replaced by a simple vacuum box of the same dimensions, shown by light-blue in Fig. 2, and metallic boundary conditions are assumed at its outer surfaces. The RFQ beam axis is shown by a blue line.

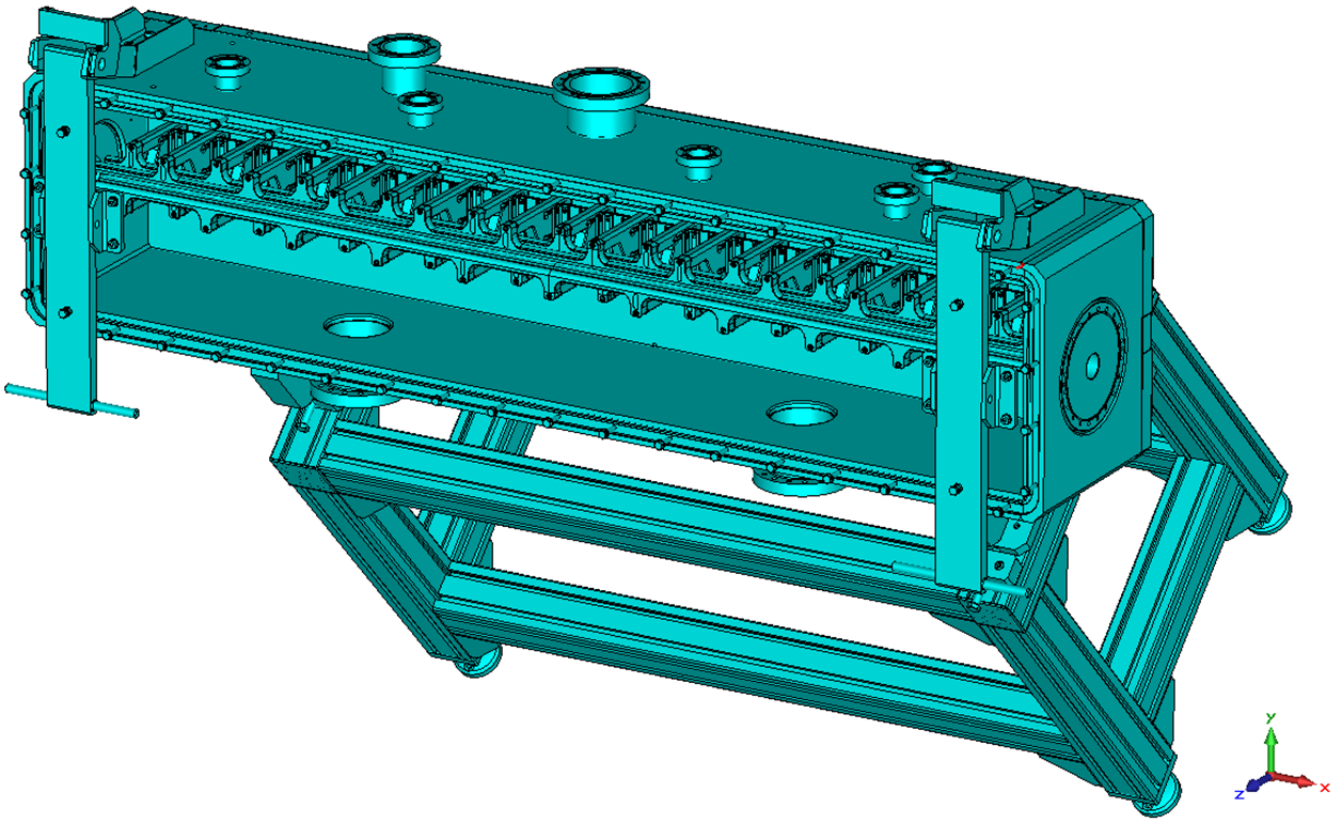

Figure 1: RFQ CAD model imported in CST. The RFQ-box lid is hidden to show the vanes and stems.

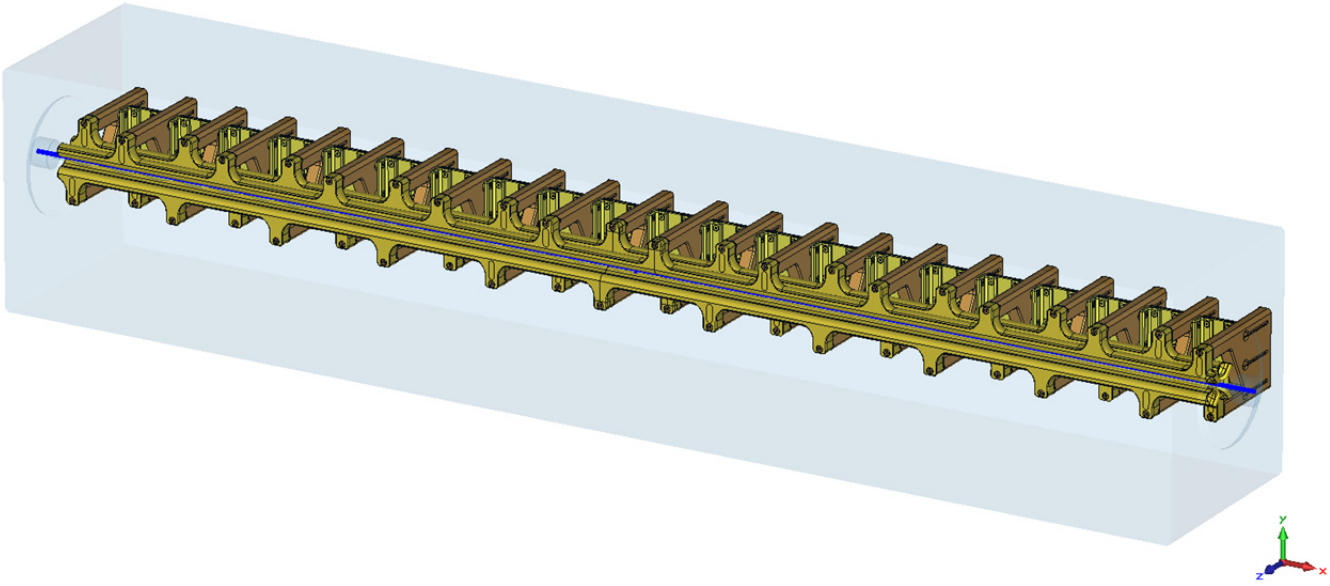

Figure 2: MWS model V of LANL RFQ with 22 stems and variable stem period.

Figure 2 shows main elements of the RFQ model: four vanes (often called ‘electrodes’ for 4-rod RFQs) with modulated profiles (copper color), their supporting stems (light-brown), and tuners (light-copper). The tuners electrically short two adjacent stems and can be moved along them (in *z* direction) to adjust the mode frequency and voltage profile (flatness) along the structure length. The tuners between stems

are seen well in Fig. 3 for the RFQ option E; the tuner details and vane modulation can be better noticed in magnified pictures in Fig. 4.

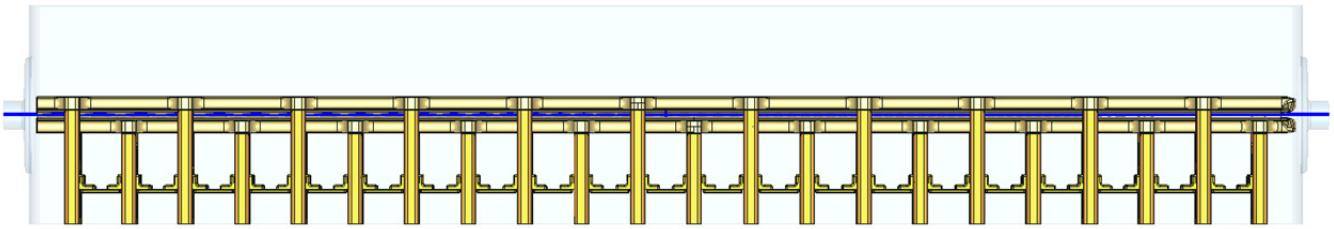

Figure 3: LANL RFQ model E with equidistant stems; side view.

One should notice that the beam (and the vane modulation pattern) goes from positive values of x to negative ones (i.e. in $-x$ direction, right to left in Figs. 1-4) in this RFQ model. The tuners are moved up very high, by 23 mm from their nominal (CAD) position, to shift the frequency up to about 201 MHz, both in V and E models. One can see that in Fig. 4 (left) that shows details of the RFQ vane ends: the tuners reached their highest possible position. Results for models V and E are similar except for a more flat voltage profile in V, which simplifies further tuning. This is why below we will only discuss model V and its modifications. One unusual feature shown in Fig. 4 is that the modulation is cut abruptly at the vane ends; there is no transition cell. In addition, a modified version of the CST model V was built by cutting the vane tips of all four vanes and by rotating the cut pieces by 90° around the RFQ axis so that the modulation patterns of two vane pairs are interchanged. We will call it model M. Figure 4 shows comparison of the two models, the original and the modified one, near the vane ends. Note the change of the vane modulation. The need for the modified model in Fig. 4 (right) will be explained later.

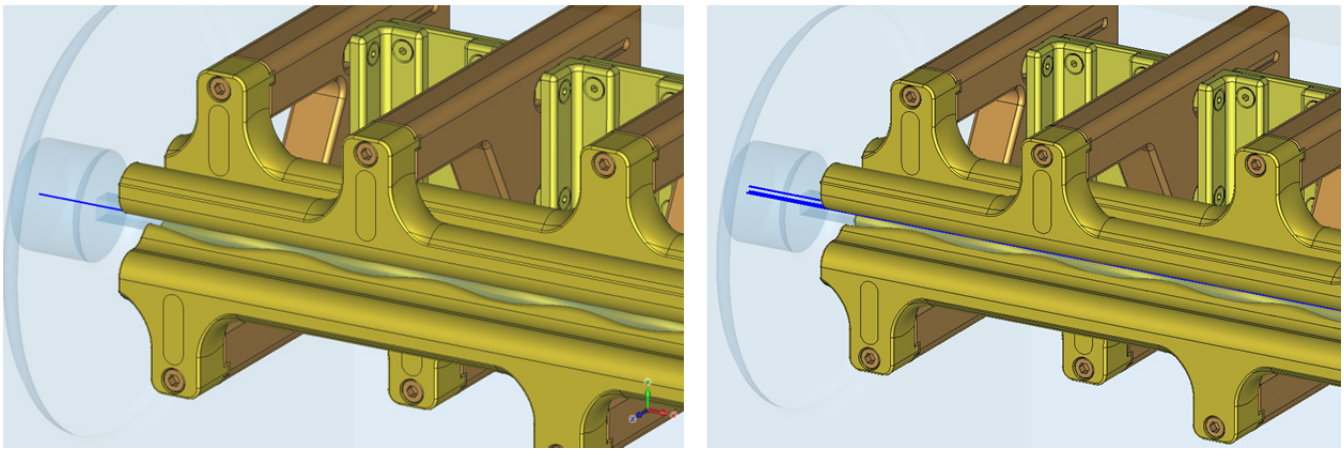

Figure 4: RFQ vane ends in the original model V (left) and in the modified one (right).

In the RFQ models we calculate eigenmode frequencies and fields using one of the MWS eigensolvers. Unfortunately, due to the complicated vane geometry, the CAD models imported into MWS are processed by ACIS with some small errors and warnings, which prevent using an efficient, well-parallelized tetrahedral solver. More tolerable hexahedral-mesh solvers, AKS or JDM, are used instead. They are not very efficient: JDM is not parallel at all, and AKS typically effectively uses ~1.8 processors. Additional tricks are required also to prepare a mesh that combines a good resolution in the regions of high fields (between the vanes) with a reasonable total mesh size. Similar to the FNAL RFQ case [5, 6], we introduced an artificial vacuum insert along the whole RFQ length that has a rectangular cross section 8 mm x 8 mm and covers the volume between the vanes (one can see it in Fig. 4), where

the mesh properties are set manually to ensure a good resolution. In some cases, two such inserts, one inside the other, are used [6]. The transverse mesh step inside the inner insert is small, no more than 0.5 mm in this case, and allowed to be twice as large in the second, outer insert. In the outside region, far from the vanes, the mesh size can be significantly larger, up to a few mm, but there are no large fields there, so the solution accuracy does not suffer. The total mesh sizes vary depending mainly on the longitudinal mesh step from about 4 million mesh points (4M) for rough models up to 22M for a fine case with two inserts and the longitudinal mesh step no longer than 1.5 mm.

The AKS solver allows mesh cells partially filled with metal, which provides a good approximation of the model geometry, but AKS does not always find a solution for this complicated layout. The JDM solver is more robust, but does not allow partially-filled cells, so often one ends up with many cells and faces filled by perfect electric conductor (PEC) in the meshing process. This distorts the metal body surfaces and may lead to unphysical spikes of the field values near such cells or faces. One has to check mesh carefully before running JDM to make sure that such PEC cells are not in the regions of main interest.

The MWS-calculated RF electric field components on the axis in the models V and M are shown in Figs. 5-6. These results were obtained with the AKS eigensolver using relatively-rough hexahedral meshes of about 11.6M mesh points. The accelerating field (longitudinal component, E_x, in red) is similar in the two models except near the vane ends. The field values here are non-scaled, in the default MWS normalization (the mode energy is 1 J). One should expect, since the vane patterns are interchanged, that the longitudinal fields in the modulated region should be in opposite phases in the two models. To make a more accurate comparison, the longitudinal fields scaled to the nominal inter-vane voltage, V_0 = 50 kV, are plotted together and compared in Fig. 7.

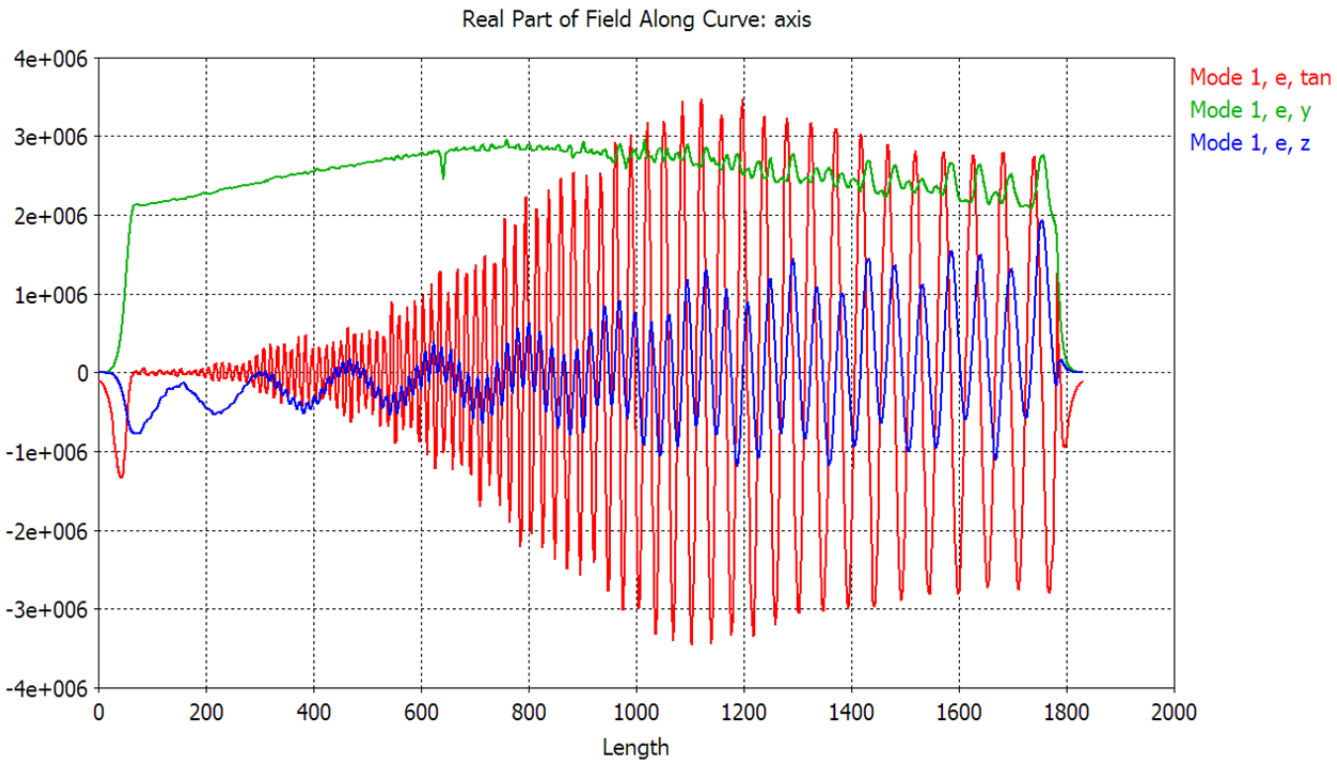

Figure 5: On-axis electric field in the RFQ model V with 22 stems.

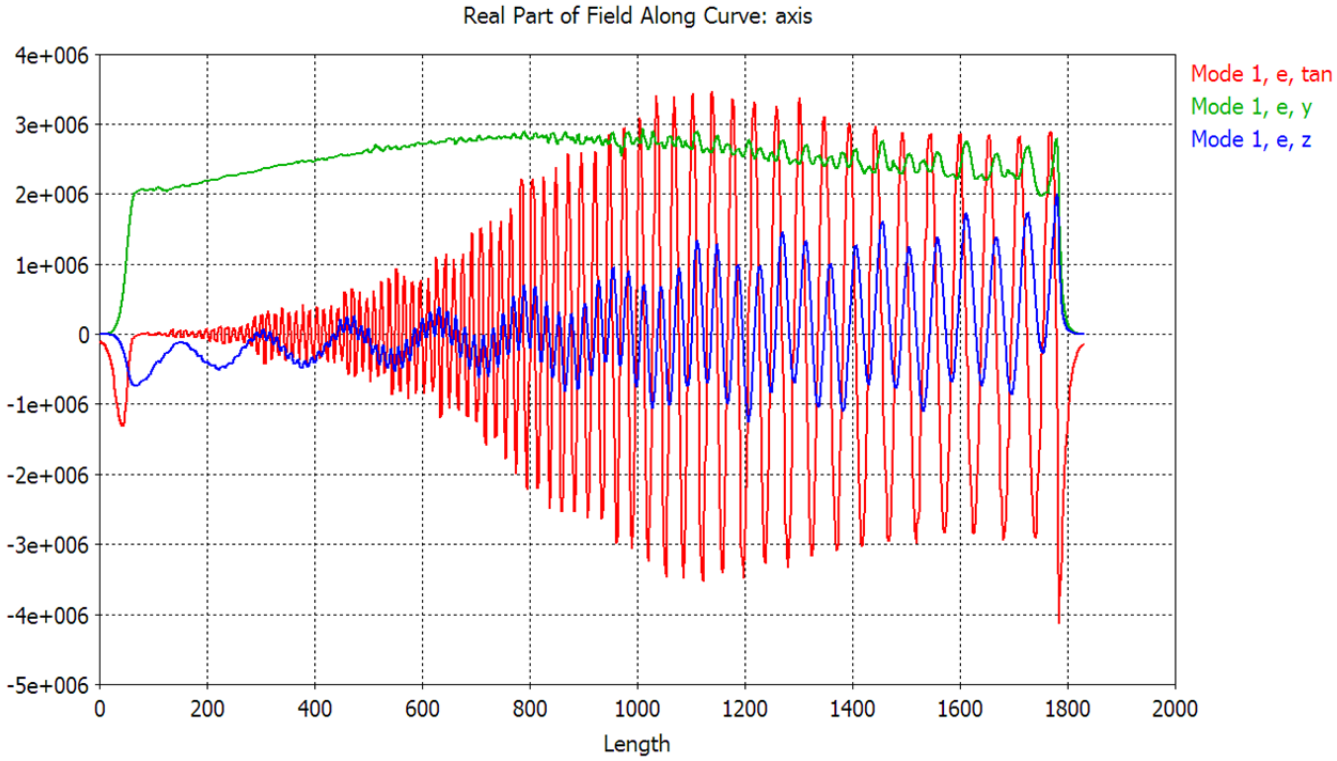

Figure 6: On-axis electric field in the RFQ model M (same as V but with interchanged modulations).

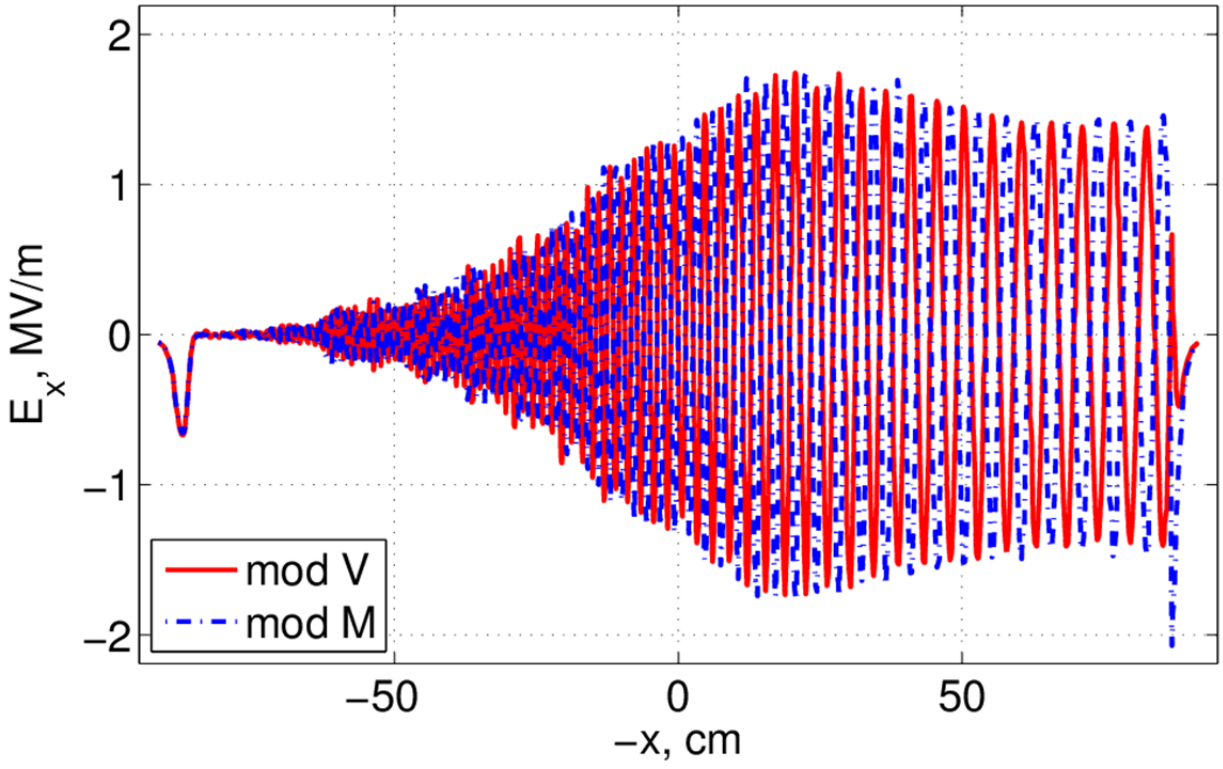

Figure 7: On-axis longitudinal electric field in the RFQ models V (red) and M (blue, dash-dotted).

As expected, the longitudinal fields have opposite phases in the modulation region, and differ near the RFQ exit. Near the entrance ($-x \approx -87$ cm), the end-gap peaks practically overlap but there is a noticeable difference near the exit end gap ($-x \approx 87$ cm), due to the interchanged modulation. In the model V, the exit end-gap field peak is suppressed, but in model M it is enhanced and has the opposite sign compared to model V.

To quickly check the RFQ output energy, we performed simplified Particle Studio PIC simulations using MWS-calculated RF fields (normalized to $V_0 = 50$ kV) injecting a linear beam of 1000 macro-particles with very low charge evenly spaced in time within 2 RF periods. The results were summarized in a short note [9]. We found that by the vane end the beam energy in both models was about the same. However, the energy drops by ~20 keV in model V after the beam passes the exit end gap. On the contrary, in model M the energy slightly increases at the exit, due to a different end-gap field, and the final energy is close to the design value, 750 keV. Actually, the low output beam energy in model V was the reason why we interchanged the vane modulations following a suggestion from A. Schempp [10]. This change was a quick fix to try: it does not require redesigning the modulation pattern but changes the end-gap fields. From the viewpoint of standard RFQ design codes, these two models are identical, and they would be identical in a classical four-vane RFQ implementation. However, in a four-rod RFQ where the end-gap effects should be taken into account [5, 6], they provide different output beams. Still the low initial frequency and insufficient tuning range had to be addressed, and the RFQ design was modified.

24 stems. A modified design with the interchanged vane profiles and 24 supporting stems was completed by IAP-Kress and received at LANL in July 2013. It has the same total length as the 22-stem version and a variable spacing between stems, 75 mm in the center and 69.5 mm between the four last stems (three periods) near each end. The CST model of the 24-stem design, with the tuned frequency and voltage profile, is shown in Figs. 8 and 9. The RFQ vacuum vessel, in light-blue, is 175-cm long (wall-to-wall), 34-cm wide, and 30-cm high (along the stem direction, z). It also includes wide recesses of radius 8.5 cm and depth 1.5 cm on the thick end and front walls, followed in the model by 5-cm-long beam pipes of radius 2 cm.

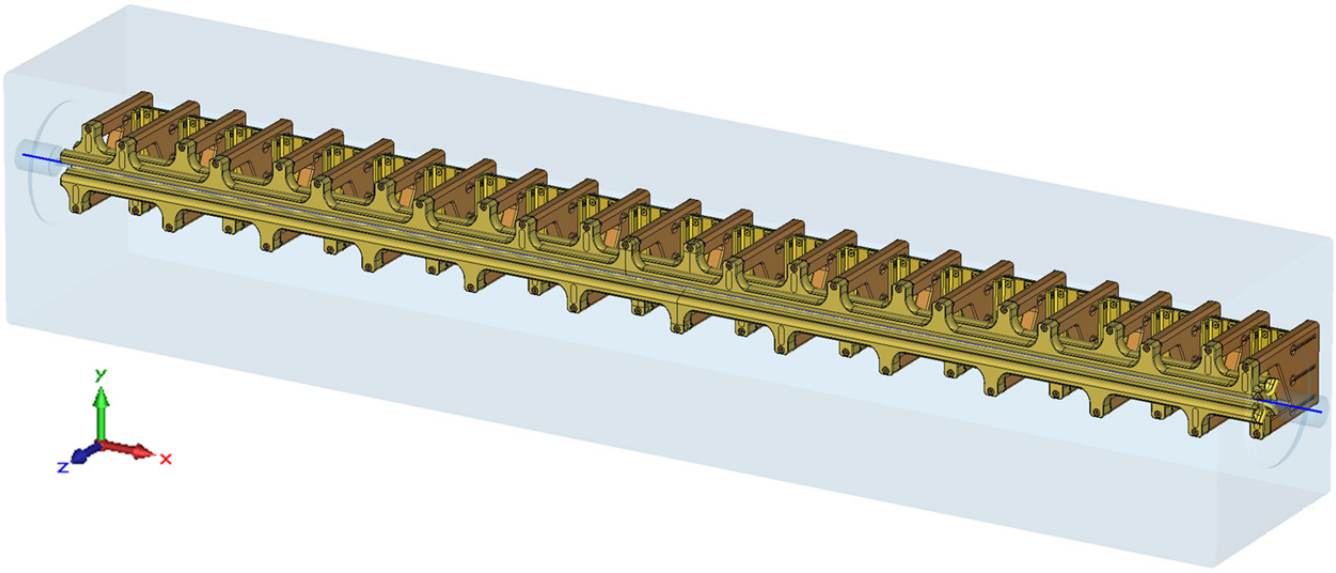

Figure 8: MWS model of tuned LANL RFQ with 24 stems and variable period.

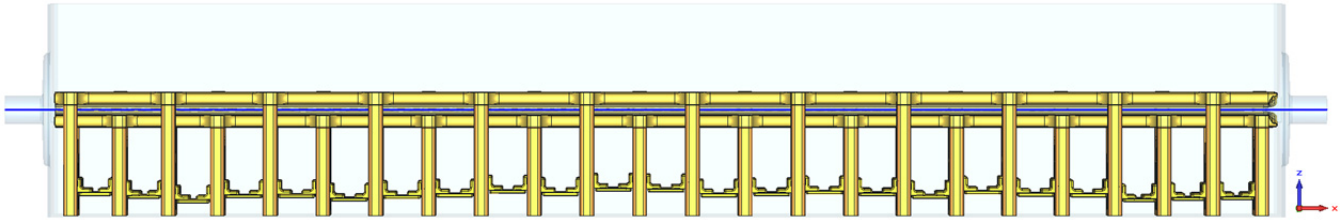

Figure 9: LANL RFQ model with 24 stems, tuned; side view.

Our RFQ model uses the CAD model coordinates: x is along the RFQ axis, see Figs. 8-9. The beam is moving in -x direction (right to left in Figs. 8-9). The MWS model in Fig. 8 was further cleaned up for calculations by removing internal cooling channels and bolts, and filling the remaining voids with metal to simplify meshing.

The mode frequencies and RF fields are calculated with the AKS eigensolver to provide more accurate surface approximations. Figure 10 shows the electric field of the RFQ working mode at 201.25 MHz. The field values should be scaled by a factor of 0.57 to provide the nominal inter-vane voltage $V_0 = 50$ kV. The unloaded quality factor of the mode is $Q_0 = 5315$ for ideal copper surfaces. The next lowest mode in the RFQ (the first longitudinal harmonics) is about 15 MHz higher in frequency.

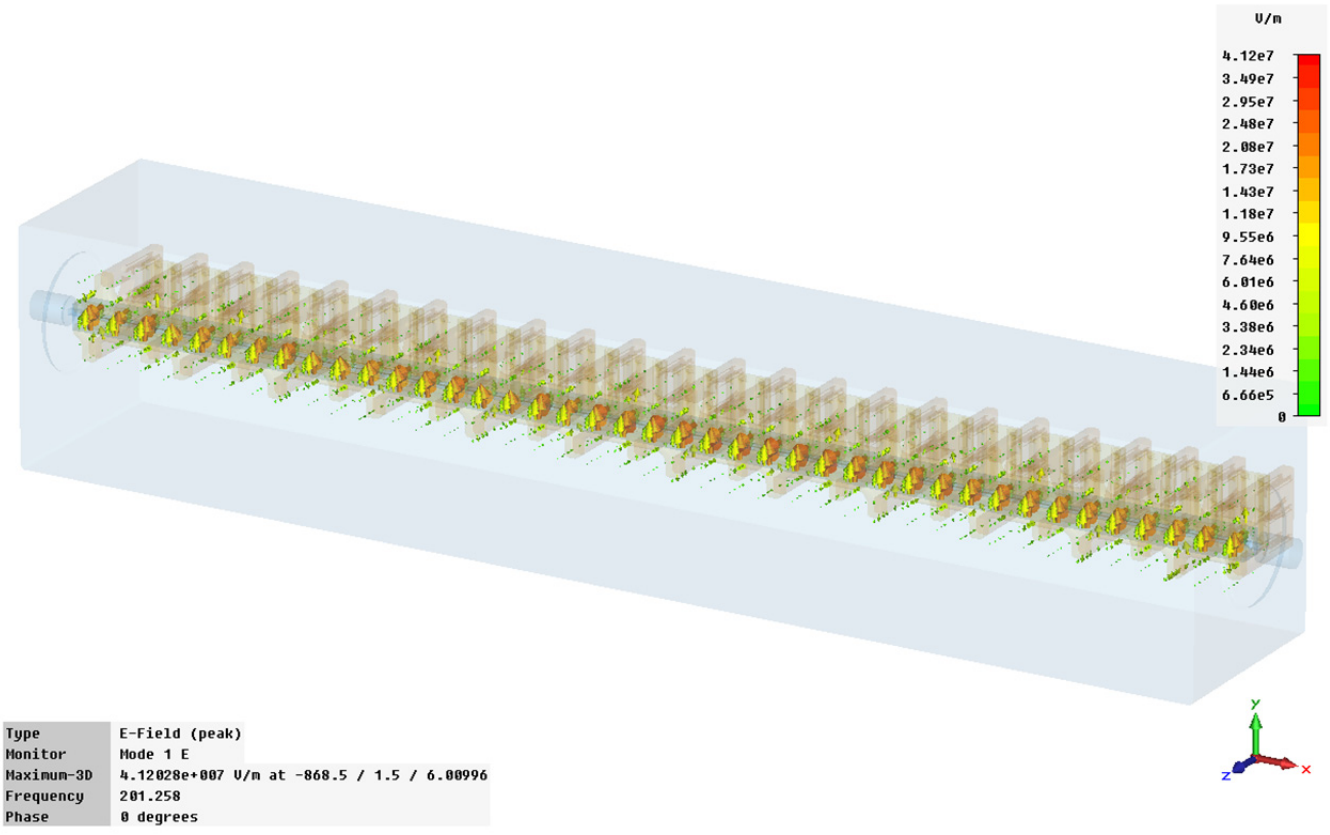

Figure 10: Electric field in the RFQ model with 24 stems (MWS normalization, log scale).

The RF fields have some interesting features resembling those found in the FNAL 4-rod RFQ, see in [5, 6]. The first is the presence of a small transverse horizontal (parallel to the ground plane) electrical-field component, E_y, on the RFQ geometrical axis, sometimes referred to as a "dipole" component. This is

due to the transverse electric fields being stronger between two top vanes than between two bottom ones – as illustrated in Fig. 11, – which results in the center of the transverse quadrupole field displaced down, to the ground plane, from the geometrical axis by 0.45 mm (to the right in Fig. 11). The shift is small but not negligible when compared to the 4-mm vane aperture. This effect is known in 4-rod RFQs designed for higher frequencies [11].

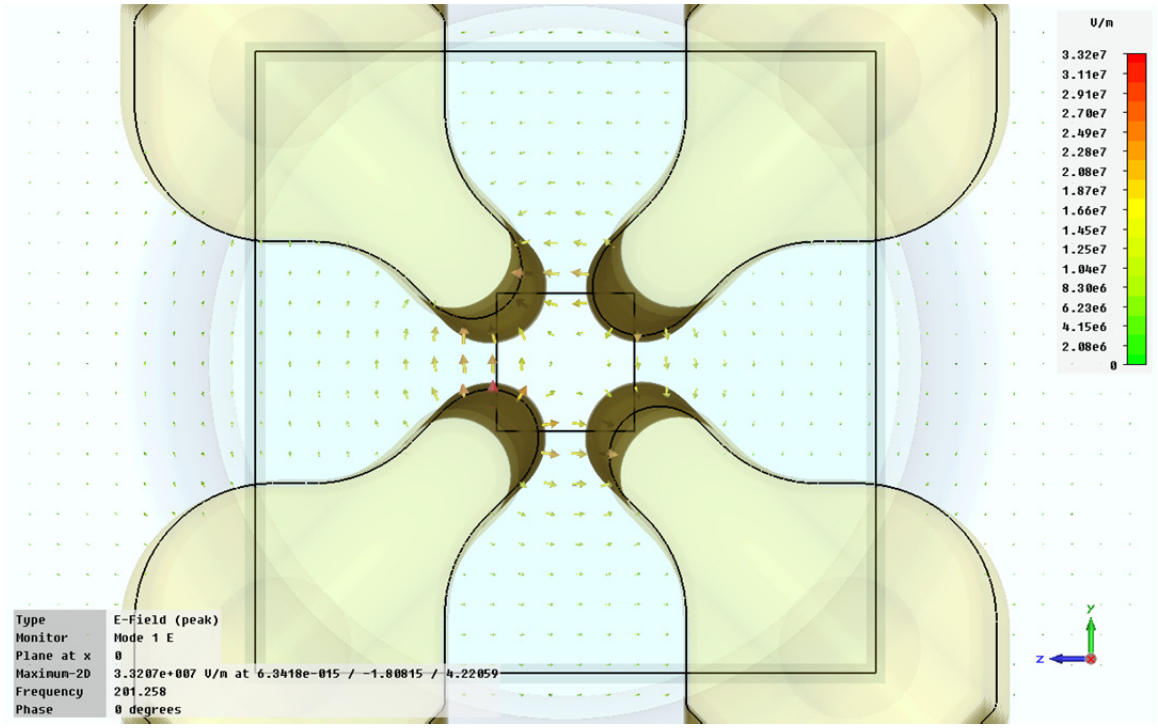

Figure 11: Electric field in the transverse cross section $x = 0$ of the RFQ. Two top vanes are on the left (at larger z), and two bottom ones – on the right.

The electric-field components on axis: longitudinal E_l ($E_l = -E_x$), horizontal E_y, and vertical (along the stems) E_z are plotted in Fig. 12 versus the longitudinal coordinate along the RFQ axis, $s = -x$. The fields are scaled to the nominal inter-vane voltage $V_0 = 50$ kV. Note that the terms "horizontal" and "vertical" here refer to the CAD coordinate system of Figs. 8 and 9, with the horizontal plane x-y being parallel to the RFQ ground plane at the bottom of the RFQ box ($z = z_{min}$), and the vertical direction is along the z-axis, to or from the ground plane. In a plot similar to Fig. 12 but along the axis shifted by -0.45 mm in z, the horizontal component E_y would be close to zero, while the other two do not change much compared to Fig. 12.

The second important feature of the 4-rod RFQ fields, as was already mentioned for the 22-stem models, is the longitudinal electric field in the end gaps that separate the vane ends from the RFQ box walls. The red curve E_l in Fig. 12 includes the RFQ accelerating field – the oscillating part – produced by the vane modulation. In addition, the curve also has two peaks, one near the entrance and another near the exit, – the end-gap bumps. The RFQ cavity extends from $s = -87.5$ cm to $s = 87.5$ cm; the vanes start at $s = -86.9$ cm and end at 86.9 cm. It would make 6-mm gaps, but the gaps are effectively wider by 1.5 cm due to the recesses cut out in the end walls and the beam pipes (one can see the recesses in Fig. 9). The wider entrance gap is the reason why the entrance peak of the longitudinal field is small. On the other hand, the large near-exit peak is caused by a special modulation cut at the vane ends in the interchanged modulation pattern of Fig. 4 (right): the modulation ends at a maximum for one pair, and at minimum for the other.

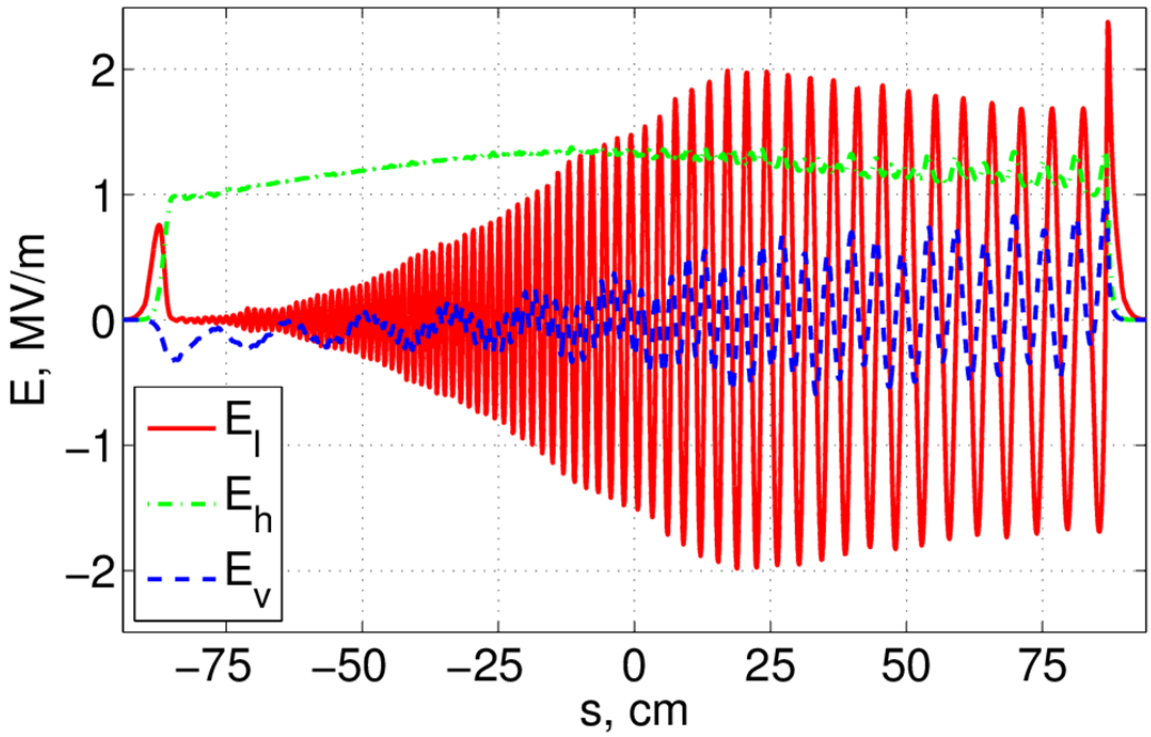

Figure 12: RF electric field components on the axis in the RFQ model with 24 stems: longitudinal (red), vertical (blue dashed), and horizontal (green dash-dotted).

In general, the end-gap bumps of the longitudinal electric field are present because of a local violation of quadrupole symmetry near the vane ends [5, 6] that occurs in 4-rod RFQs or 4-vane RFQs with windows. They would vanish in perfectly symmetric structures like a classical 4-vane RFQ. In 4-rod RFQs there are always two short vane pieces in one plane (they are connected to the nearest stem), and two long pieces in the other (perpendicular) plane, which are connected to the next stem that is one stem-to-stem distance further, see in Fig. 4. Moreover, in the end-gap areas there are transverse field components in addition to the usual quadrupole ones. Under some circumstances the end-gap fields, which are neither predicted nor taken into account by standard RFQ design codes, can change the exiting beam parameters such as energy and emittances [5, 6].

One important requirement for the RFQ operation is having a flat inter-vane voltage along the structure. After the RF fields are found with an eigensolver, the inter-vane voltages are calculated in the post-processing by integrating the electric field along short (36 mm) segments between the vanes in the middle of each RFQ period (i.e. in the middle between two stems). The segments are placed outside the RFQ aperture, at 18 mm from the RFQ axis, to minimize numerical noise. Previously [5, 6] we used for voltage calculation very short segments, 10 mm, at 5 mm from the axis, that included only a few mesh points between the vane tips. The results were much noisier even though the segments were positioned on the surface of an inner vacuum insert to be aligned with the mesh for higher integration accuracy.

The relative voltages, calculated at the midpoints of all 23 full periods, are presented in Fig. 13 for two cases: with all tuners at the same height, only the frequency is tuned to 201.25 MHz (“initial”) and after tuner adjustments in the MWS model (“tuned”). Even for the initial profile, the voltage was reasonably flat, within ±5% of the average value; this is due to the variable stem spacing. When all 23 tuners are moved together, varying their spacing h up from the ground plane, the frequency sensitivity is df/dh = 0.75 MHz/mm. The initial frequency tuning was achieved by shifting all the tuners up by Δh = 3.75 mm

from the nominal CAD file positions. The tuner positions for the "tuned" case are shown in Fig. 9: the tuners are at different heights but generally rather low compared to the 22-stem case, cf. Fig. 3. The positions are adjusted in the MWS model to make the inter-vane voltage flat within ±1%. In the shown tuned case of Fig. 9, the additional displacements of individual tuner plates range from -9.5 mm to 8 mm. The frequency tuning range is comfortably sufficient in this design.

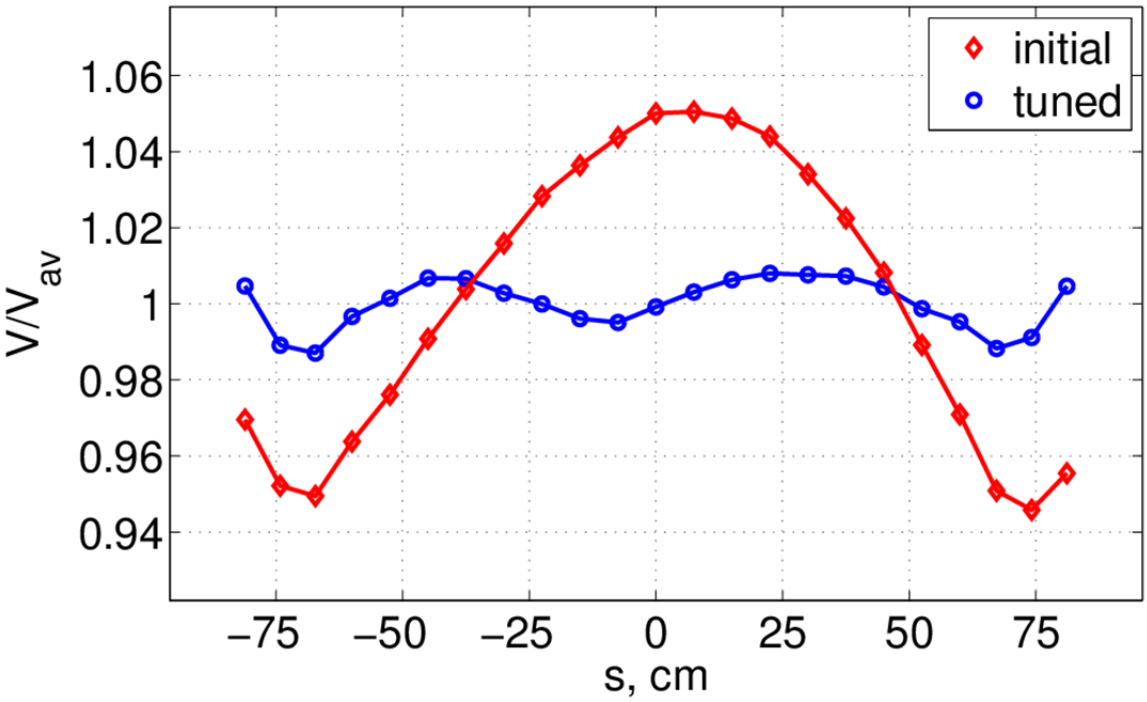

Figure 13: Voltage profile along the RFQ structure.

The calculated maximal field E_{max} = 23.5 MV/m ($1.6E_K$) for the nominal inter-vane voltage V_0 = 50 kV is reached near the vane exit end. We use the fields calculated in the tuned case for our macro-particle simulations, and the related heat flux for thermal-stress analysis.

3. Beam dynamics simulation with Particle Studio PIC solver.

The RF fields (E, H) of the RFQ working mode calculated with the MWS can be imported into the CST Particle Studio (PS). In the process, we scale the MWS field solution to the required inter-vane voltage, e.g. to the nominal value of V_0 = 50 kV for the LANL RFQ. The next step is to provide an initial macro-particle distribution for the particle-in-cell (PIC) solver. There are a few built-in particle distribution types in the PS. However, we will use externally-created realistic particle distributions and import them into PS. The process was described in [6]; here we briefly summarize it. An external (macro-)particle distribution is prepared as a text file (*.pit) with the number of lines equal to the particle number. Each line contains 10 particle parameters: coordinates x, y, z, momenta $(\beta\gamma)_x$, $(\beta\gamma)_y$, $(\beta\gamma)_z$, particle mass, charge, macro-particle charge, and time. It is convenient to choose particles being injected in a fixed plane transverse to their direction of motion. In our case, it will be at $x = x_{max}$ for particles moving in the negative x direction; the initial particle RF phases are translated into different injection times. The macro-particle charge q is defined by the beam current I and chosen number n of macro-particles within one RF period. In the case of an RFQ working at frequency f with CW beam injection, $q = (I/f)/n$.

One simple initial distribution for checking the RFQ output energy was already mentioned above in Sec. 2. It was a set of particles at a fixed energy of 35 keV injected along the same line (e.g., on axis) and distributed evenly in time within $2T$, where T is one RF period, $T = 1/f = 4.97$ ns for $f = 201.25$ MHz. Such a linear distribution includes all initial RF phases in determining the average output energy. Having two RF periods guaranties that one gets at least one full "bunch" (filled RF bucket) in the output beam. For the output energy check, it is also convenient to set the macro-particle charge very low to eliminate space-charge effects.

More realistic initial distributions should be matched to the RFQ for a design current. Such distributions can be generated using beam dynamics codes, e.g. PARMILA [8]. Larry Rybarcyk has developed a procedure to generate matched distributions for the FNAL RFQ [5]. Using matched beam parameters at the RFQ entrance (at the beginning of the vanes), a CW particle distribution at the injection energy for a given current and transverse emittance is generated. The generated particles are evenly distributed in phase within one RF period. After that the particles are back-traced from the match plane to the injection plane, again with PARMILA. One should note that back-tracing works accurately only for very low currents when space-charge forces are negligible. For higher currents, one needs to choose somewhat different initial distributions in the injection plane that evolve into the matched one at the vane entrance with space-charge effects taken into account. Eventually the PARMILA-generated distribution is reformatted into the PS input format (*.pit) with a simple Matlab script, repeated for N RF periods, and shifted in space, so that the macro-particles are injected in the RFQ at $x = x_{inj}$ within the time interval $[0, NT]$.

The CST Particle Studio PIC solver is a general PIC code. Unlike specialized beam dynamics codes [8, 12], it does not have built-in diagnostics of beam parameters like rms size, emittance, energy spread, etc. However, in PS one can set particle monitors: in configuration space, 3D monitors record particle positions within simulation volume at specified times and 2D ones record particle positions and momenta when the particles cross a fixed plane; there are also various phase-space monitors. Information recorded by such monitors can be extracted and post-processed to obtain the usual beam dynamics parameters. As an illustration of PS simulations, Fig. 14 shows macro-particles in the 24-stem RFQ model recorded by a 3D monitor at the moment $t = 405$ ns after the injection start. The 3D monitor was set to record particles every 1 ns. In this particular PS run, a 35-mA CW proton beam was injected at 35 keV during $N = 10$ RF periods (total 10x10K particles). At the shown moment a few leading particles already exited the RFQ structure, and the total number of macro-particles at this moment is 97.4K. The particle energy is indicated by color; the energy scale is on the right. Figure 14 shows the beam after it was bunched in the buncher section and illustrates how the formed bunches are being accelerated to 750 keV in the accelerator section near the RFQ end. There are about 9000 macro-particles in each bunch, many times more than between bunches. The low-energy tail particles (dark-blue) are not captured in the RF bunches; there are a few thousand of such particles. Some of these low-energy particles will be lost off axis in the RFQ, and some will come out of RFQ off energy; the latter ones will likely be lost in the following beam transport.

Figure 15 shows the number of macro-particles N in the RFQ model with 10x10K beam injected versus time t for three different currents. The red curve corresponds to the case shown in Fig. 14 at $t = 405$ ns. The number increases linearly until all 100,000 particles are injected ($10T = 49.7$ ns), then it remains constant or start to decrease slightly as some particles are lost (more losses for higher currents). The first particles reach the RFQ exit shortly after 400 ns, and after that one can see steps on the falling slop due to the exiting bunches. The total number of exiting bunches is 11 or 12.

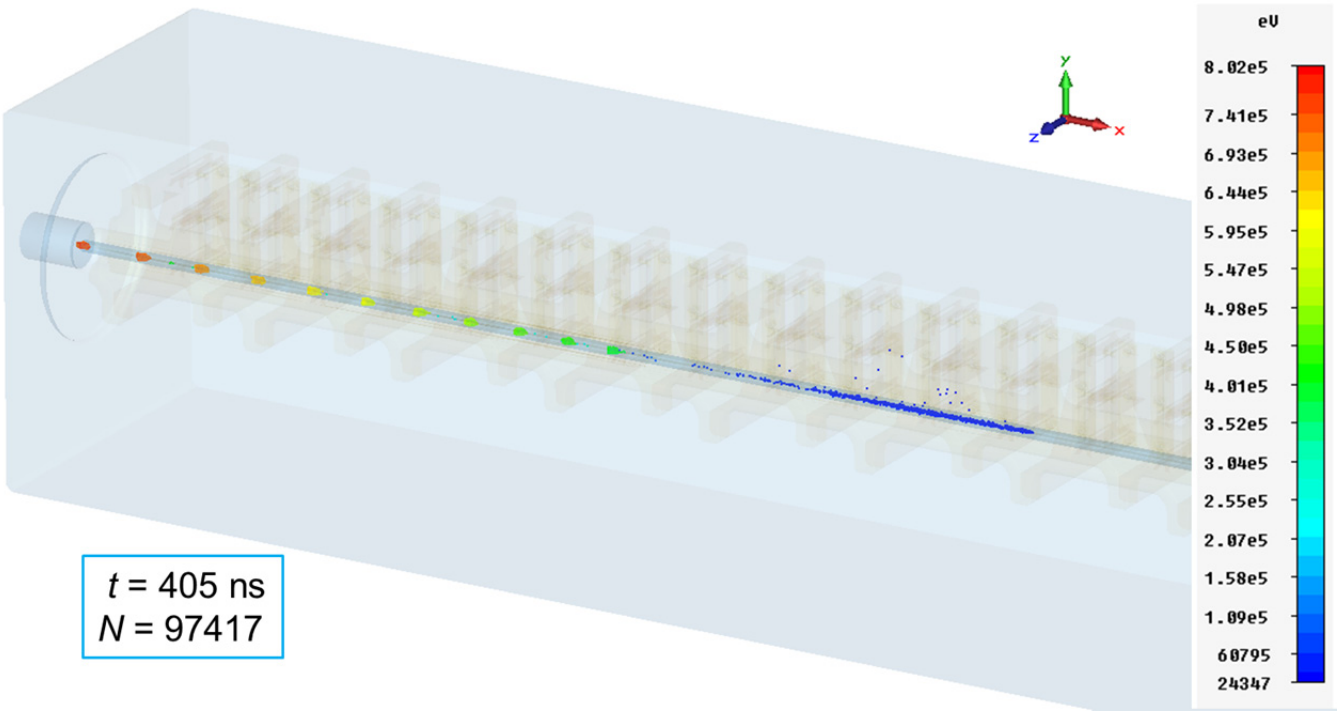

Figure 14: Particles approaching the exit in the RFQ model at t = 405 ns for 10x10K beam with current of 35 mA. Color indicates particle energy.

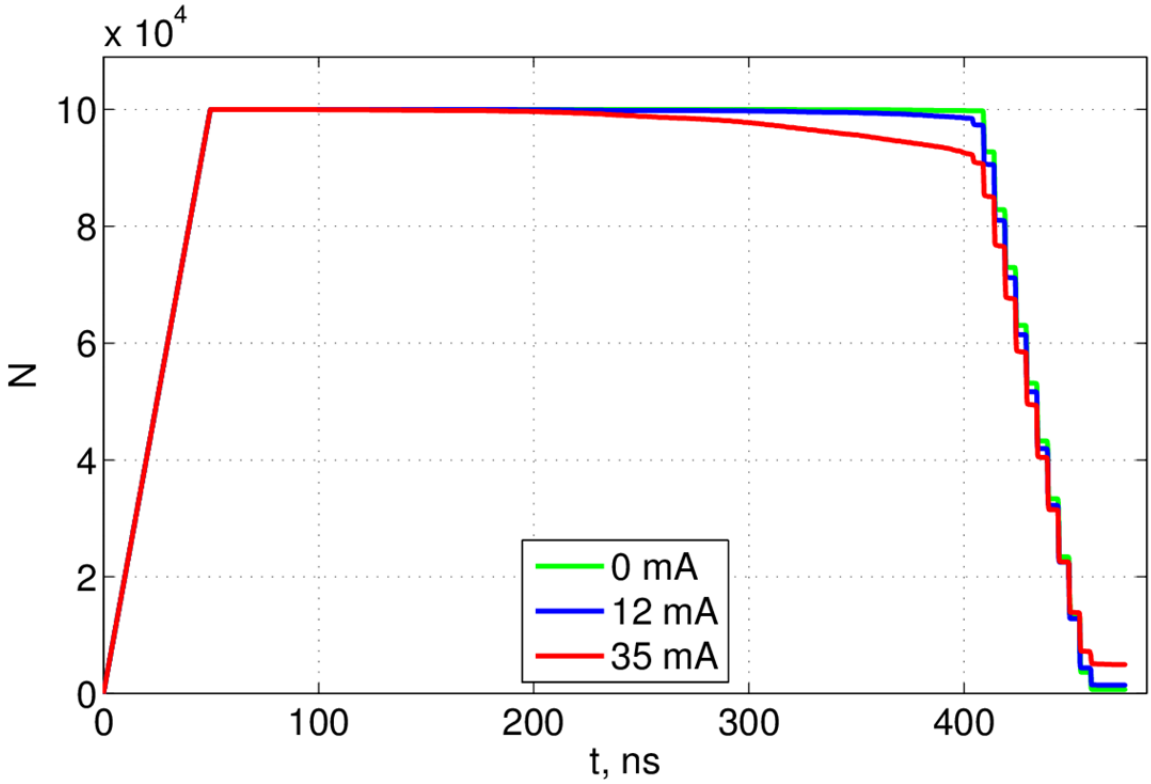

Figure 15: Number of particles in the RFQ model versus time for three different currents with 10x10K CW beam injected.

The first and last bunches are usually partially filled because the train edges fall into two adjacent RF buckets. This is the only splitting effect at low currents. For higher currents, there are also effects of space charge in the longitudinal direction that push particles at the head and tail of the injected beam into the adjacent one or two RF buckets.

Another way to look at what happens in the PS simulation is with phase-space snapshots. In Fig. 16, five subsequent phase-space snapshots of the longitudinal phase space x-W (coordinate-energy), starting at t = 406 ns with 1-ns step, are overlapped. Each one is shown in different color, and together they cover about one RF period. It should be reminded that the beam moves in the negative x direction in this model. One can see the bunch formation (11 bunches, the last one is somewhat hollow) and acceleration along the structure as well as the low-energy particles not captured in bunches and falling off energy. The vanes (and their modulation) end at x = -869 mm and the RFQ box end wall is at x = -875 mm. The bunch energy increases as it moves to the vane's end, changes slightly in the extended end gap (gap plus wall recess, x from -869 mm to -890 mm), and then stays constant in the exit beam pipe (x < -890 mm). One can notice that the energy change near the RFQ exit in the model is rather small, and the bunch average energy is close to the design value, 750 keV. More accurate results are obtained by analyzing data from 2D particle monitors in the exit beam pipe. The bunch spacing near the RFQ exit at β = 0.04 (750 keV) is $\beta\lambda$ = 6 cm, where λ = 149 cm is the RF wavelength; cf. the bunches snapped at a particular moment in time, i.e. of the same color, in Fig. 16.

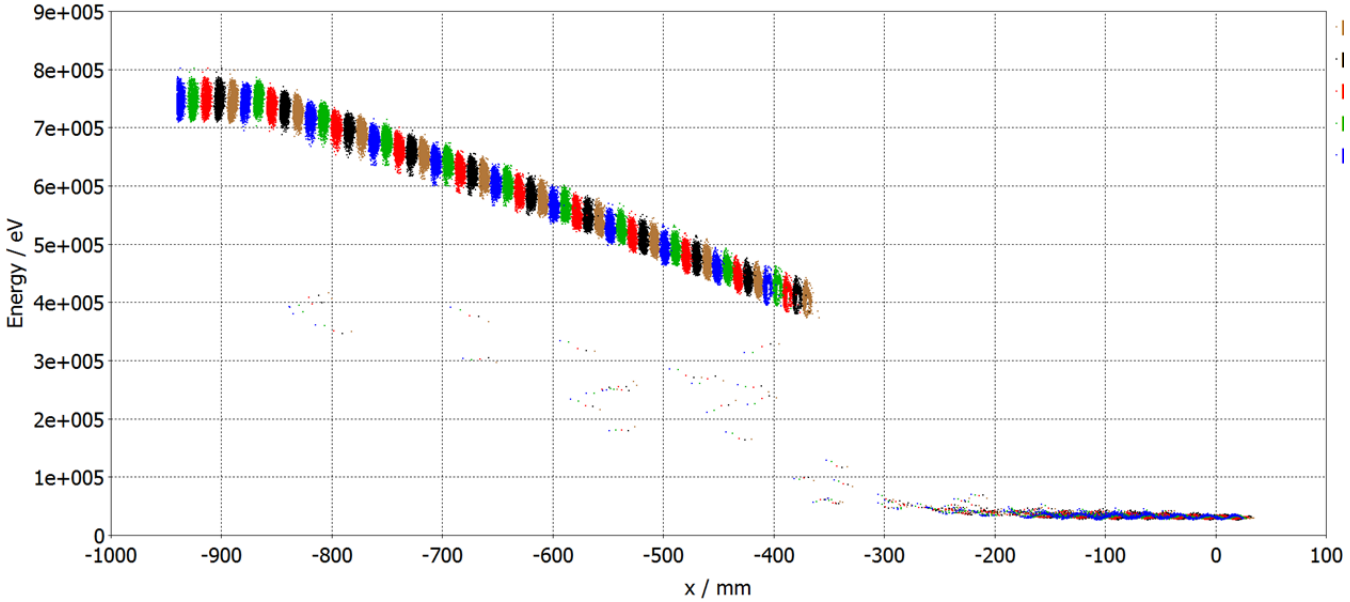

Figure 16: Five overlapping snapshots of the longitudinal phase space with 1-ns step starting at t = 406 ns for 10x10K input beam at 12 mA. The particles move right to left, in the negative x direction.

Figure 17 shows the number of macro-particles N in the LANL RFQ model versus time t with 100x10K beam injected. The number increases almost linearly (without small particle losses it would be exactly linear) till the moment when the first particles reach the RFQ exit, ~400 ns. After that there is a flat top for about 85 ns during which the CW beam injection still continues, with small zigzags corresponding to exiting bunches. By 497 ns the injection is completed, and the number of particles starts to decrease; small steps on the falling slop are due to the exiting bunches. Again, the total number of exiting bunches is slightly more than 100 mainly due to longitudinal space-charge effects that push particles at the head and tail of the injected beam into adjacent RF buckets. Three cases are considered: currents of 12 mA and 35 mA at the nominal inter-vane voltage V_0 = 50 kV, and 35 mA at the voltage increased by 20%,

to 60 kV. The total number of macro-particles in PS simulations is above 800,000 in these cases. One can notice a small deviation from the linear growth for 35 mA due to particle losses along the structure while the beam is still being injected.

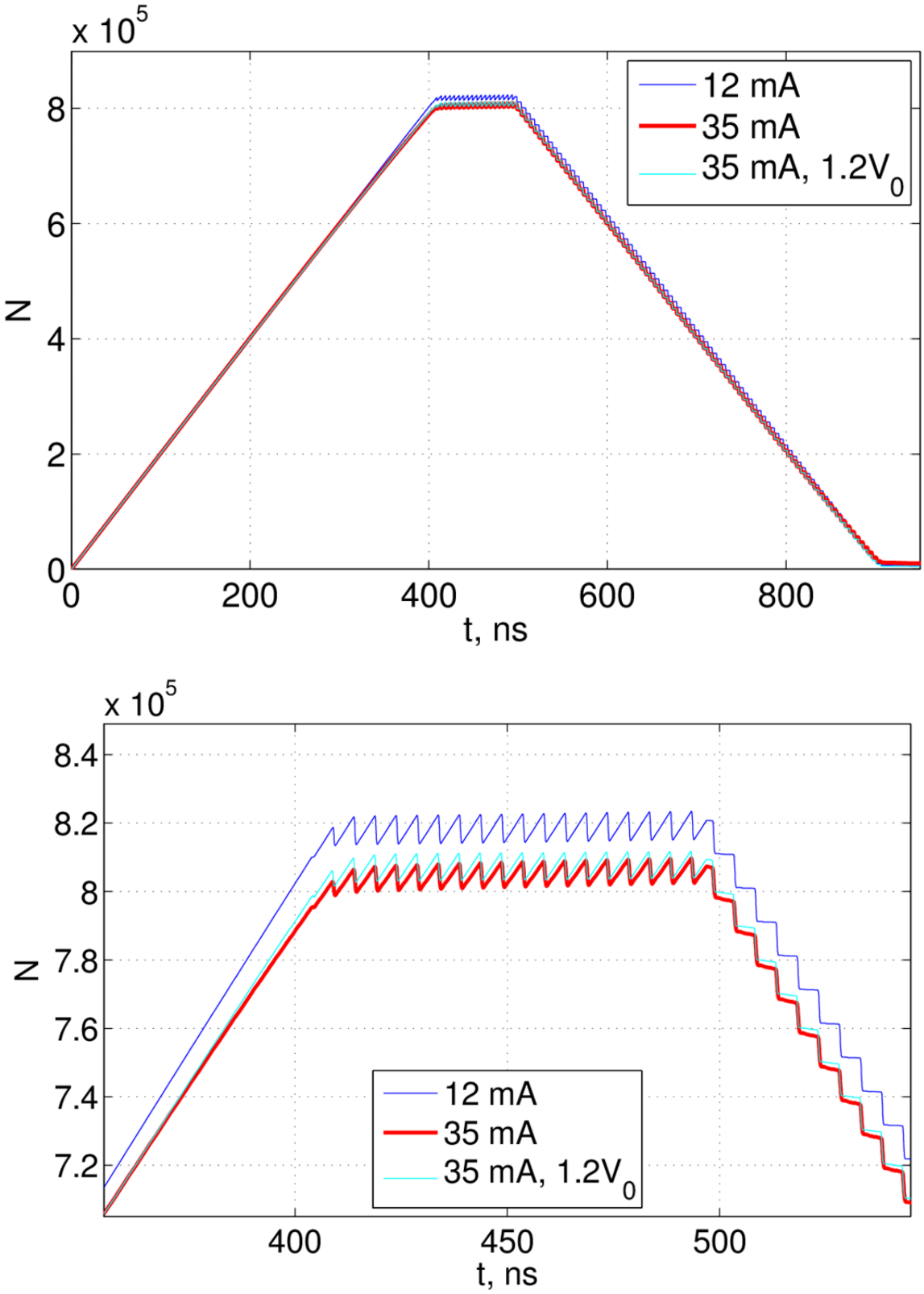

Figure 17: Number of particles in the RFQ model versus time with 100x10K CW beam injected for three cases (top); details of curves near the flattop (bottom).

A snapshot of macro-particles in the RFQ model with a long injected CW proton beam, 100x10K , is shown in Fig. 18 for the current of 35 mA and the increased inter-vane voltage, $V = 1.2V_0 = 60$ kV, at the moment $t = 455$ ns after the injection start. It corresponds to the mid-flattop of the cyan curve in Figs. 17, and the total number of macro-particles in the structure at this moment is about 805K. Again, as in Fig. 14, the particle energy is indicated by color. The injected CW beam (dark-blue, on the right) is initially converging due to the preceding low-energy beam transport (LEBT) that provides beam matching to the RFQ. The beam is bunched in the buncher section, and the created bunches are accelerated to 750 keV in the RFQ accelerator section. One can notice that the PS model in this case is cut transversely, compare to the full-volume models in Figs. 14 and 8 above. This is done to reduce the total number of the mesh points in the PS model, while keeping the dense mesh in the beam region, and allows us to speed up PS simulations significantly. Still a PS run with 100x10K beam takes about 37 hours on a PC with dual Intel Xeon E5-2687W eight-core processors at 3.1 GHz. The cut PS model uses the same external MWS-calculated RF fields as the full model, but only their part that covers the smaller model volume, where the beam propagates. However, the wakefields generated by the beam in the cut volume can be different from those in the full model. We have compared results for the full and cut models with 10x10K beams for different currents, and found no noticeable differences in the exit beam parameters even at 35 mA, which leads us to conclude that wakefield effects in our RFQ are negligible. One should also mention that standard beam-dynamics simulations with PARMELA [8] or BEAMPATH [12], even when they use imported MWS-calculated fields, restrict the simulation region to a very small volume within the RFQ aperture.

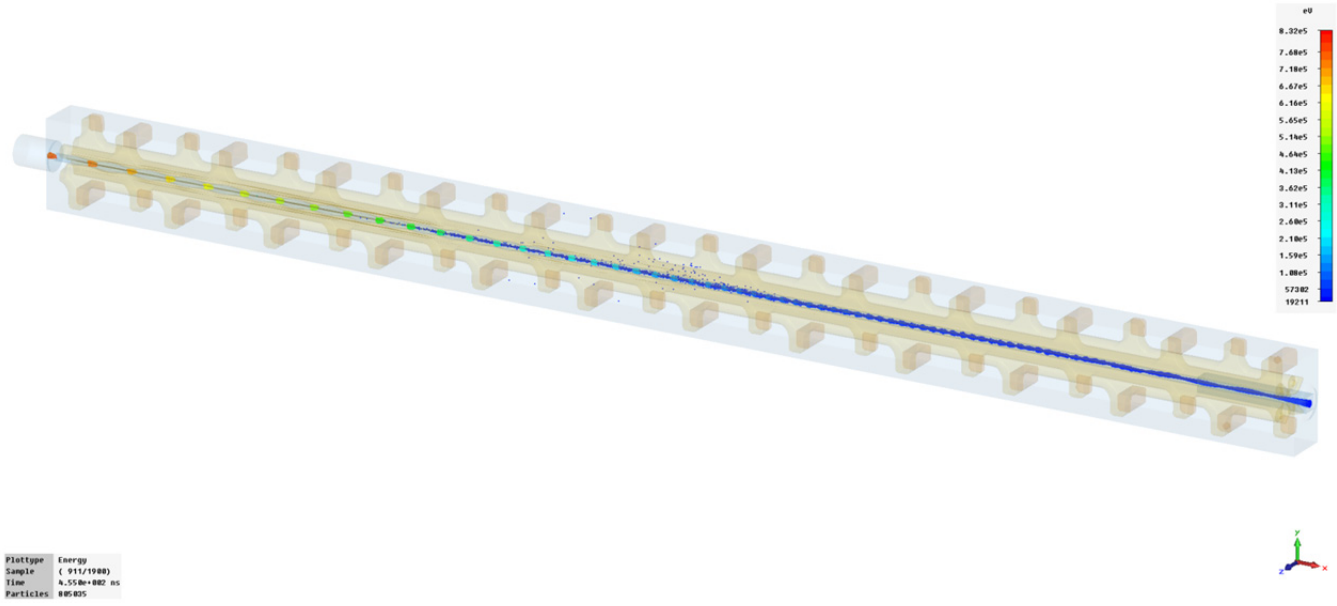

Figure 18: Particles in the transversely-cut RFQ model at $t = 455$ ns with 100x10K beam for 35 mA and $V = 1.2V_0 = 60$ kV. Color indicates particle energy.

The PS PIC 2D particle monitors record particles crossing a fixed plane within specified time intervals. The recorded information can be exported into a *.pit file that may be used either for post-processing or as an input for follow-up simulations. We set 2D monitors in the exit beam pipe – in the transverse plane at $x = -900$ mm or -920 mm – with transverse boundaries -10 mm $< y, z <$ 10 mm and a short time step of 0.01 ns. We post-process 2D monitor results with a Matlab script that reads the recorded *.pit files and manipulates the data to calculate the RFQ exit-beam parameters.

As an example of such post-processing, Fig. 19 plots the energy of exiting particles recorded by a 2D monitor at x = -900 mm from PS simulation of the RFQ model with a matched CW proton input beam at 35 mA injected over 10 RF periods (10x10K) – the case illustrated above in Fig. 14. The right picture in Fig. 19 essentially shows the top part of the left one, including all macro-particles except those whose energy W < 700 keV; there were only 164 such particles out of 85768 in the left picture, i.e. less than 0.2%. We introduce the energy cut, ±50 keV around the design energy 750 keV, to take into account the acceptance of the structures following the RFQ.

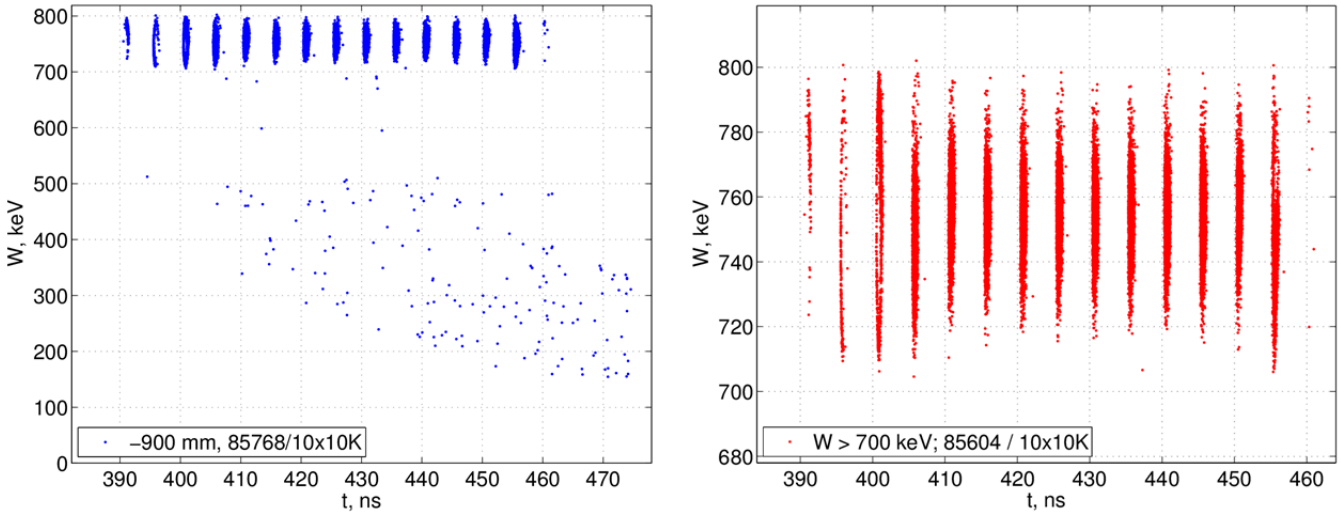

Figure 19: Results from 2D monitor at x = -900 mm in the RFQ model with 10x10K 35-mA beam: all exiting particles (left) and only those with energy above 700 keV (right).

The exiting particles form more than 10 bunches due to space-charge pushing particles into the adjacent RF buckets. We select only 8 subsequent bunches starting from the one near t = 411 ns and usually analyze 4-6 central ones as less distorted by edge effects. The total number of particles in the 8 central bunches is 69817, i.e. the RFQ effective transmission rate for this current can be estimated as 69817 / 80000 = 0.873. Details of bunch population and energy for this case are presented in Figs. 20.

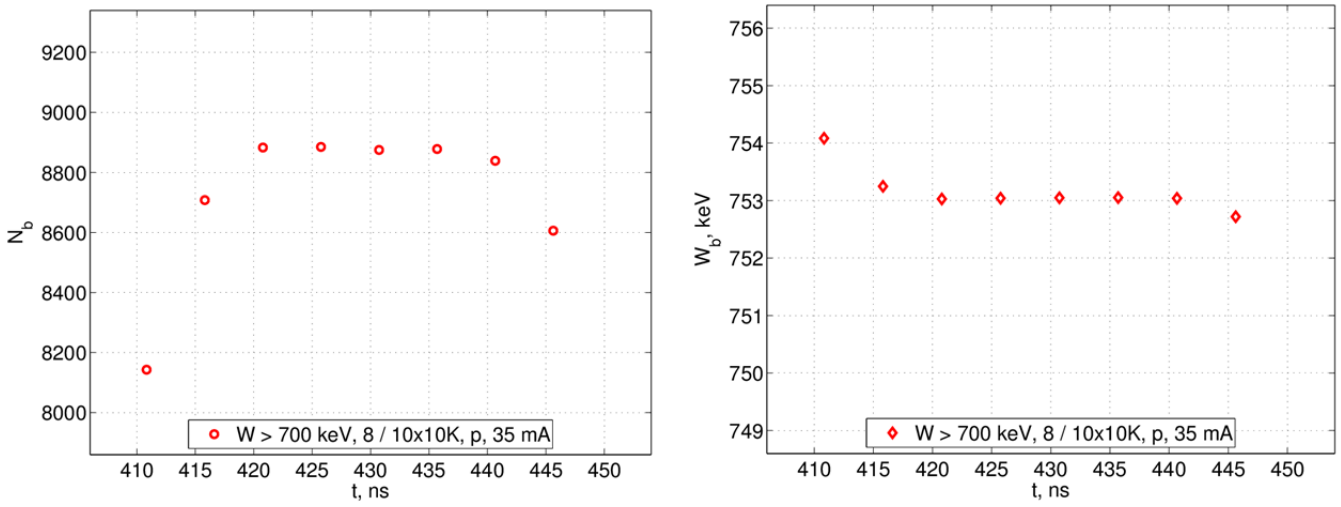

Figure 20: Bunch population (left) and average energy (right) versus time for 8 central bunches with 10x10K 35-mA beam.

Figure 20 (left) shows the bunch population for 8 central bunches, and Fig. 20 (right) plots the average bunch energy. One can see that for this current only 4-5 bunches in the middle have approximately the same number of particles, $N_b \approx 8900$, and energy, 753 keV. Since the maximal possible number of exiting particles per RF period is 10K in our PS simulations, assuming no losses and stationary state, the bunch population plot in Fig. 20 gives us the RFQ transmission rate, which should probably be ≈0.89 in this case. The lower the current in simulations with 10x10K input beams, the closer are parameters of all 8 central bunches. An example in Fig. 21 presents the bunch populations for two cases: 12 mA and a very low current, "0 mA". The transmission rates are 0.97 and 0.99, correspondingly.

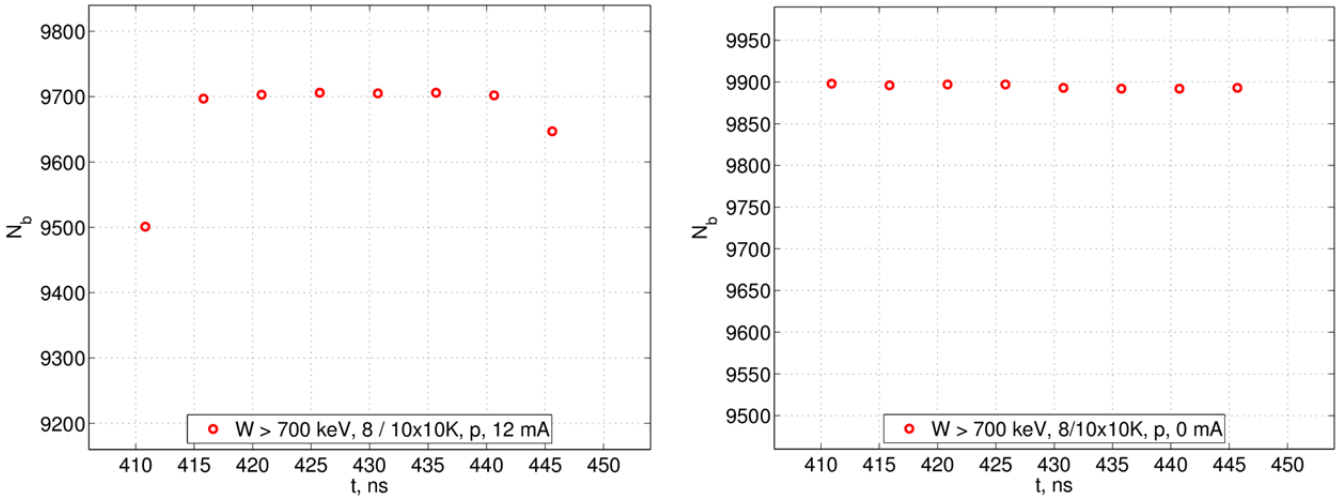

Figure 21: Number of particles in 8 central bunches from PS simulations with 10x10K input beam at 12 mA (left) and very low current (right).

For a few cases, PS simulations were also performed with longer 100x10K beams. Analyzing 2D-monitor results from such runs, we consider only 80 central bunches while discarding more than 10 bunches near each end of the bunch train. The results for bunch energy and population are shown in Fig. 22 for 35 mA with the increased inter-vane voltage $V = 1.2V_0 = 60$ kV.

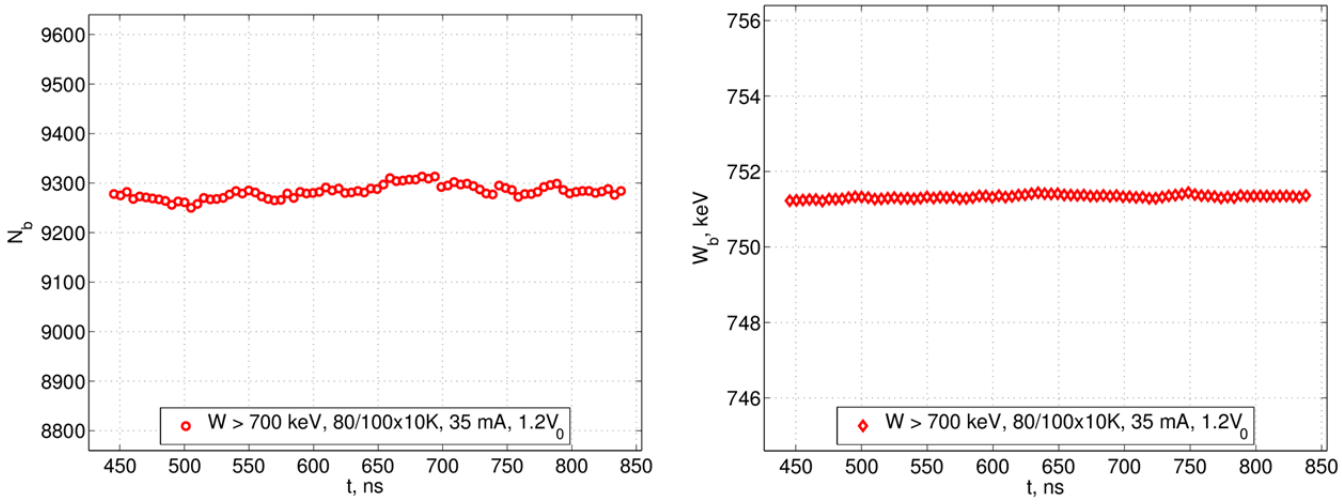

Figure 22: Parameters of 80 central bunches from PS simulations with 100x10K input beam for 35 mA with $V = 1.2V_0 = 60$ kV: number of particles per bunch (left) and average bunch energy (right).

There are small variations of the bunch population N_b, probably of statistical nature, but the average energy is practically constant. One can notice that the transmission for this current, 35 mA, increases to ≈0.93 from 0.89 due to the voltage increase.

The beam emittances after the RFQ are important parameters. It should be emphasized that the transverse emittances must be calculated in the lab frame coordinates, i.e. in the lab horizontal and vertical planes that contain one pair of RFQ vanes each, to avoid coupling between two transverse planes of the beam independent betatron oscillations. The lab system is rotated 45° around the RFQ axis with respect to the coordinates used in our model, see Fig. 1 and imagine that the RFQ support table stands on a floor. The lab r.h.s. coordinate system (h, v, s) is related to our model coordinates (x, y, z) as follows:

$$h = \frac{z - y}{\sqrt{2}}; \quad v = \frac{y + z}{\sqrt{2}}; \quad s = -x.$$

The importance of calculating transverse emittances in the proper coordinates has become clear after comparison of PS results with results of BEAMPATH simulations – the credit goes to Yuri Batygin, [13] – where the imported MWS-calculated RFQ fields and the same initial beam distributions as in PS were used. Figure 23 plots the transverse emittances of the 80 central bunches from the PS simulations with 100x10K 35-mA beam, calculated both in the proper coordinates (left) and in the model coordinates (right; incorrect results due to mixing of two transverse oscillations). The initial transverse normalized rms emittances were chosen to be 0.2 π mm·mrad in both planes. Unfortunately, incorrect preliminary results for the emittances were reported in [7]. One should clarify the notations used in the emittance plots in Fig. 23 (right): the "horizontal" transverse emittance – in the plane parallel to the RFQ ground plate – is denoted ε_y and corresponds to the coordinate system in Fig. 1, but for the "vertical" transverse emittance (in the plane along the stems) we used ε_x, though it would be ε_z if we followed Fig. 1, where x is the longitudinal coordinate.

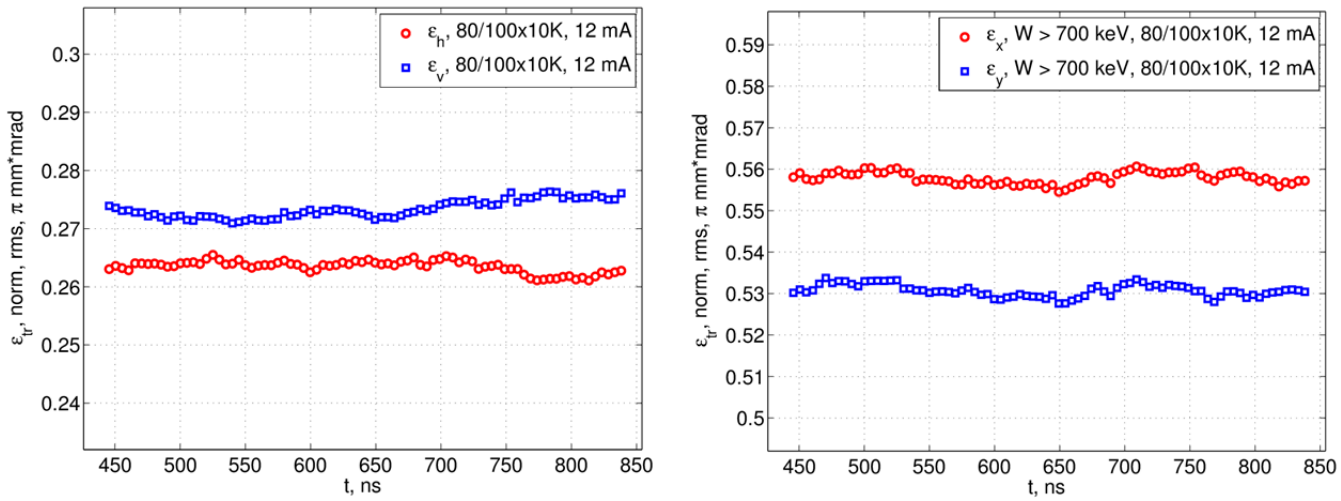

Figure 23: Transverse normalized rms emittances for 80 central bunches with 100x10K 12-mA input beam calculated in rotated (lab) coordinates (left) and in RFQ model coordinates (right, incorrect).

It is interesting to compare the transverse emittances for two cases with the same current, 35 mA, but different inter-vane voltages, $V = V_0 = 50$ kV and $V = 1.2V_0 = 60$ kV, cf. Fig. 24. The emittances are just a bit higher in the last case, where they also become equal in both planes.

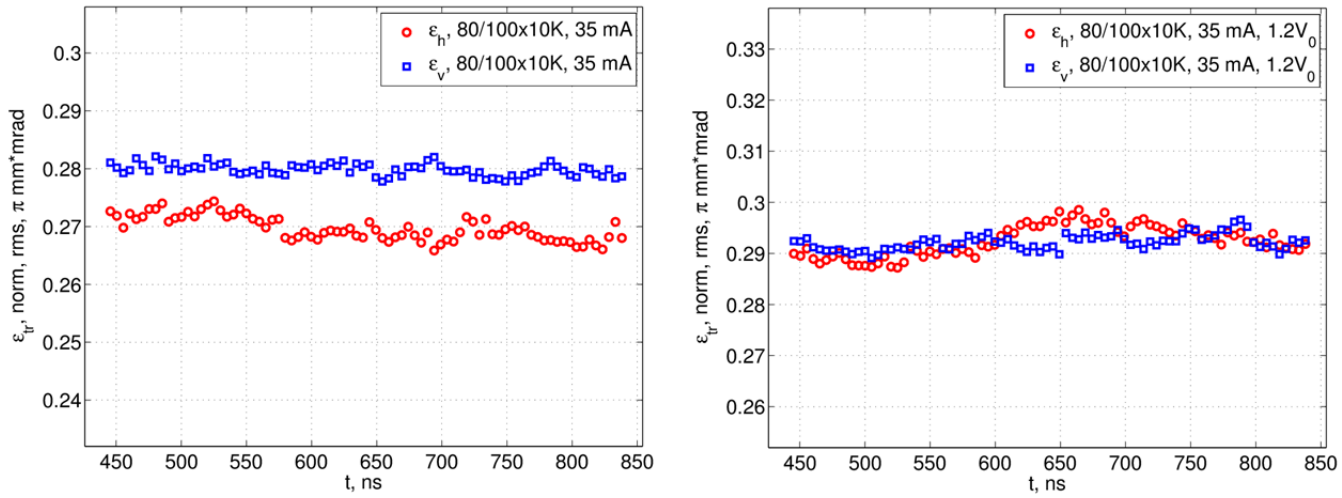

Figure 24: Transverse normalized rms emittances for 80 central bunches with 100x10K 35-mA input beam at the nominal inter-vane voltage (left) and at 20% higher voltage (right).

In the above PS simulations the initial particle distributions were injected centered on the RFQ beam axis. We checked what happens when the same distribution is centered on the field symmetry axis, which is parallel to the RFQ geometrical axis but displaced from it by -0.45 mm in *z* (vertically, along the stems), see in Sec. 2. The results are do not change much except the transmission is slightly higher, by about 1-2%, and emittances are a bit smaller in the field-symmetry centered cases; the same was observed previously for the FNAL RFQ [5, 6]. Results of various PS runs for the LANL RFQ model are summarized in Table 1. The table lists some initial simulation parameters: the beam current I, normalized r.m.s. transverse emittance ε_t, and inter-vane voltage V. In all cases, the initial beam is injected with energy 35 keV. The output beam parameters in the table are transmission, the beam average energy W, horizontal and vertical normalized r.m.s. transverse emittances (ε_h and ε_v), and longitudinal r.m.s emittance ε_s, both in keV·deg and mm·mrad.

Table 1: Results of PS PIC simulations with different initial beams.

Initial parameters			Output beam parameters					
I, mA	ε_t, π mm·mrad	V, kV	Transm.	W, keV	ε_h, π mm·mrad	ε_v, π mm·mrad	ε_s, keV·deg	ε_s, π mm·mrad
0	0.2	50	0.99	756	0.25	0.235	128	0.56
12	0.2	50	0.97	756	0.255	0.27	85	0.37
24	0.2	50	0.94	754	0.25	0.25	79	0.35
24*	0.2	50	0.95	753	0.24	0.235	76	0.34
35	0.2	50	0.88	753	0.26	0.27	87	0.38
60	0.2	50	0.68	753	0.28	0.30	96	0.42
0	0.2	60	0.995	746	0.27	0.24	138	0.60
12	0.2	60	0.975	754	0.265	0.26	113	0.50
35	0.2	60	0.93	751	0.29	0.29	104	0.46
12	0.021	50	0.985	753	0.112	0.112	51	0.22
24	0.03	50	0.96	754	0.15	0.15	53	0.23
35	0.06	50	0.91	753	0.185	0.195	66	0.29
35	0.125	50	0.90	754	0.215	0.225	77	0.34

* Initial distribution is shifted (centered on the field symmetry axis, not the RFQ geometrical axis)

Apart from the results listed in Table 1, there are other interesting characteristics of the RFQ output beam such as its transverse size and angular distributions, energy distribution, etc. For example, in the process of the FNAL RFQ commissioning for production it was found [14] that up to 10 mA were lost after the RFQ in a short Medium-Energy Beam Transfer (MEBT) to DTL. The problem was traced to the beam exiting RFQ at an angle of 1-2° vertically (in the lab frame). We then used the existing data from previous PS runs for the FNAL RFQ to confirm that such an effect was also observed in simulations [5, 6]. Figure 25 shows the angular distributions of all 85661 exiting particles in the LANL RFQ model with 35-mA 10x10K beam. This case is similar to the one in Figs. 19-20 but has a slightly better matched initial distribution; this is why the total numbers of exiting particles differ for two cases with the same current. Here the horizontal angular distribution has the average value $\langle\theta_h\rangle = -0.44°$; the vertical distribution is a bit wider but with the similarly small average angle of $\langle\theta_v\rangle = 0.46°$.

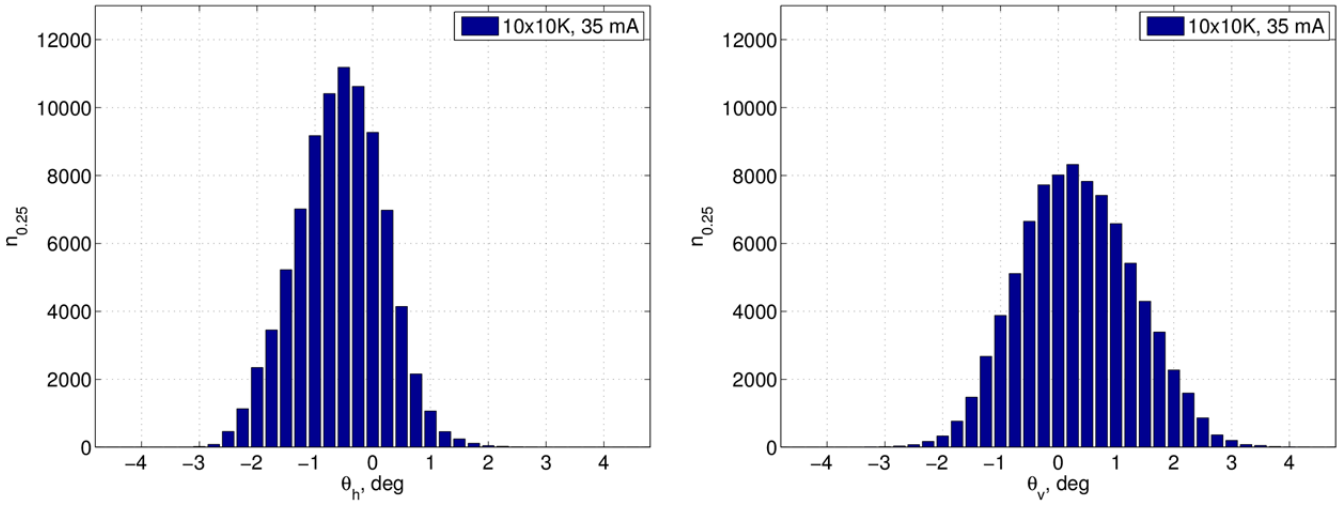

Figure 25: Histograms of particle exit angles (bins of 0.25°) in the LANL RFQ model – horizontal (left) and vertical (right) – at x = -920 mm from PS simulations with 10x10K 35-mA input beam.

For the same case of the 35-mA 10x10K beam, Fig. 26 shows a plot of positions of all exiting particles in the x = -920 mm plane (left) – it includes low-energy particles, cf. Fig. 19, and the energy distribution in the 8 central bunches. The rhombic shape of h-v plot in Fig. 26 is typical for all the cases run in PS.

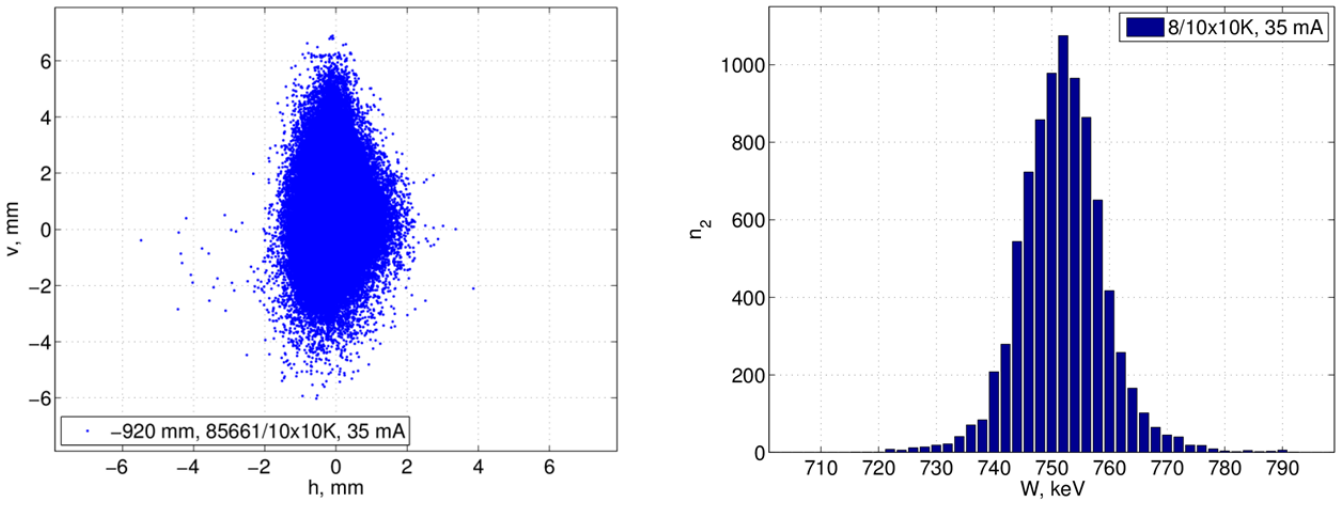

Figure 26: Particle exit position (left) and energy histogram for 8 central bunches (right, bins of 2 keV) at x = -920 mm for 10x10K 35-mA input beam in the LANL RFQ model.

In conclusion, we summarize some computational details. RFQ fields are calculated with MWS eigensolvers as described in Sec. 2. Better surface approximation and field quality are obtained with the AKS eigensolver that allows partially filled (TST) mesh cells. In our RFQ model, good quality fields for tuning were computed with moderate meshes of 12-14M mesh points. The computations take 20-24 hours on a 4-year-old PC with dual quad-core 3.33-GHz Xeon W5590 processors and 24 GB of RAM ("old PC"), or 14-18 hours on a PC with dual Intel Xeon E5-2687W eight-core processors at 3.1 GHz and 64 GB of RAM ("new PC"). The RF fields for PS simulations were computed with fine meshes of 21.35M mesh points. These computations took 62 hours on the old PC, and ~51 hours on the new one. As was already mentioned, the AKS solver is not very efficient and effectively uses only ~1.8 processors.

We import the MWS-computed RF fields, properly scaled, into the PS PIC solver. The mesh used in the PS can be different from the one employed in the MWS to calculate fields with eigensolvers. We typically use in PS runs the same mesh density in the beam region as in MWS, and less dense mesh outside that region; this results in 13.7M mesh for the RFQ PS full-volume model, cf. Fig. 14. The CST PIC solver is well parallelized; the computer memory was not a limitation in our simulations. Still, a PS run of the full model with 10x10K input beam takes 30-32 hours on the new PC (and at least 1.5 times longer on the old one). The PIC solver does not allow TST mesh cells, so some mesh cells and faces, usually the ones near complicated metal boundaries, end up being filled by perfect electric conductor (PEC) in the meshing process. This does not influence the quality of imported MWS fields, however; as long as such PEC cells or faces are not in the beam path, the PIC results can be trusted. As we already discussed above in Sec. 3, a transversely cut PS model was also used, to speed up PS runs, after a few comparisons showed good agreement with the full-model results. The cut model keeps the same dense mesh in the beam region, but the total mesh size is only 4M due to its small transverse size, see Fig. 18. A typical PS run time, with the same RF fields, is reduced to 8-9 hours for the cut model with 10x10K beam. Still a PS run with long 100x10K beam takes ~37 hours even in the cut model because the PIC run time is proportional to the chosen length of simulation time, 950 ns in this case, and also increases as the number of particles in simulations becomes larger. The amount of disk space to store the run results depends directly on the number of particles, mainly due to huge 3D particle monitor files. If 3D particle monitor is set to take a snapshot every 0.5 ns, the disk space needed to store a PS run with 100x10K beam is ~70 GB. An animated sequence of such snapshots makes a good movie (~1 GB) illustrating the beam dynamics in the RFQ. After the movie is recorded (with HyperCam), the particle monitor file (*.ppp, 60 GB in the above case) can be deleted without affecting other results.

Finally, other beam-dynamics codes were used to compare with the CST Particle Studio results for the LANL RFQ. The scaled RF fields in the beam region, which was restricted transversely by a square h x $v = 2a$ x $2a$, where $a = 4.7$ mm is the RFQ aperture without vane modulations, were imported from MWS into the standard beam-dynamics codes PARMELA [8] or BEAMPATH [12]. The same initial beam distributions as in PS were used in these beam dynamics simulations. The results from both codes are in agreement with those in Table 1. The most detailed comparison was performed with BEAMPATH [13]. The values for transmission and transverse emittances from BEAMPATH turn out to be slightly higher than from PS. This could be expected since BEAMPATH applies a larger aperture than the real RFQ aperture with the vane modulations as in the PS CAD-based model. In a sense, PARMELA and BEAMPATH simulations use an extreme version of the transversely cut RFQ model that was described above for PS; the particle tracking and space-charge calculation are completely different from PS, of course.

4. Thermal-stress analysis.

From the MWS analysis of the LANL RFQ, the total dissipated power in the structure for ideal copper surfaces is 77 kW for the nominal inter-vane voltage V_0 = 50 kV at 100% duty. It is distributed as follows: 55% on stems, 28% on vanes, 17% on tuners, and less than 0.5% on the RFQ-vessel inner surface. The distribution of the surface-current amplitude on the inner elements is shown in Fig. 27. The field and current values are in the default MWS normalization, and should be multiplied by a factor of 0.57 to correspond to V_0 = 50 kV. The maximal surface magnetic field and the highest power flux are at the stems near the RFQ end, at the location where the short stem leg connects to the stem cut.

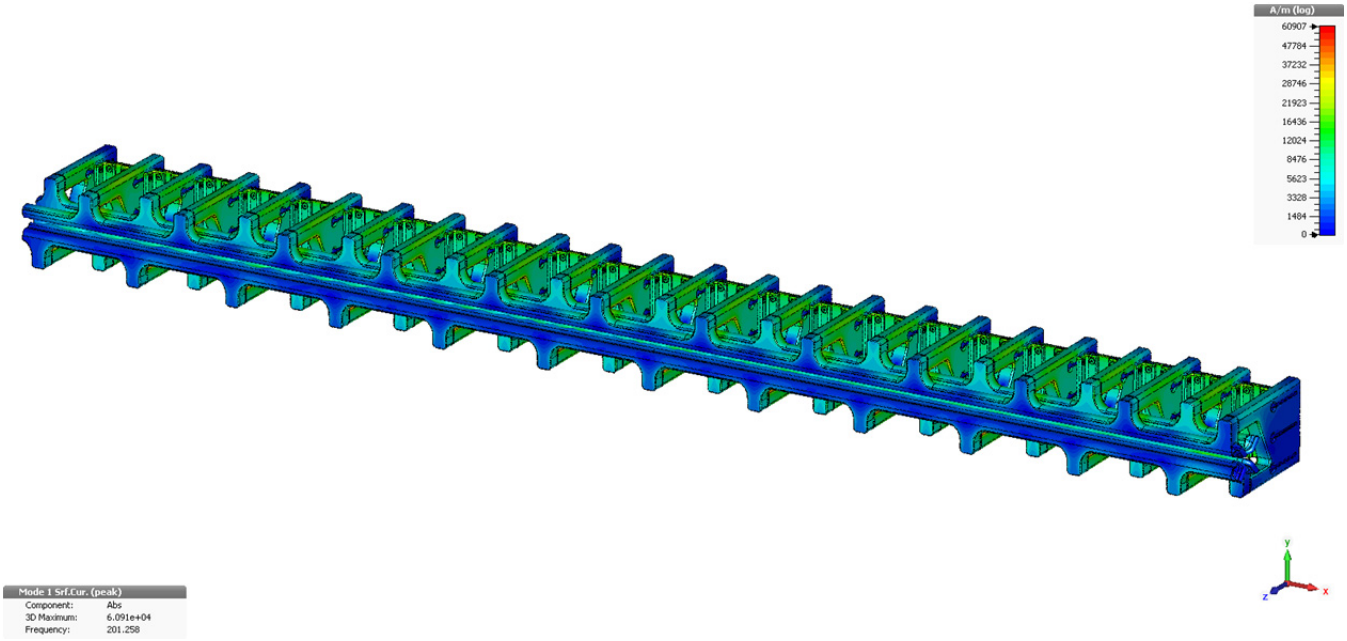

Figure 27: Surface-current distribution in the 24-stem LANL RFQ from MWS (magnitude, log scale).

Since the RFQ will operate at noticeable duty factors, up to 15%, the structure requires adequate cooling. It will be provided by water running through cooling channels. Each stem has a separate inverse-V-shaped cooling channel, see in Fig. 28. In addition, there are cooling channels inside vanes (also shown in Fig. 28), which are connected through a few stems to pipes under the ground plane. A detailed thermal-stress analysis of the RFQ model was performed with ANSYS [15]. We developed a procedure [16] to transfer surface-loss power data calculated by MWS to the finite-element (FE) engineering codes, e.g. ANSYS, as a thermal load. The important feature of the procedure is that the MWS fields are extracted not exactly at the cavity surface points but with a small offset into the cavity along the normal to each surface FE (triangle) out of the center point of the FE. This approach allows to reduce errors in the surface fields introduced by the hexahedral MWS meshes, as well as in the cases when the central points of the surface FEs are located below the metal boundary, inside convex metal walls, see [17] for details.

The ANSYS thermal analysis was performed by Eric Olivas for short sections of the RFQ tank both near the middle and near the end of the RFQ at various duty factors, up to 100%. In the thermal computations realistic contact copper-copper conductivities between vanes, stems, and tuners were taken into account. The calculated temperature distribution in a structure slice near the RFQ exit is shown in Fig. 28 for the duty of 18% (15% plus additional heating due to realistic surface conductivity).

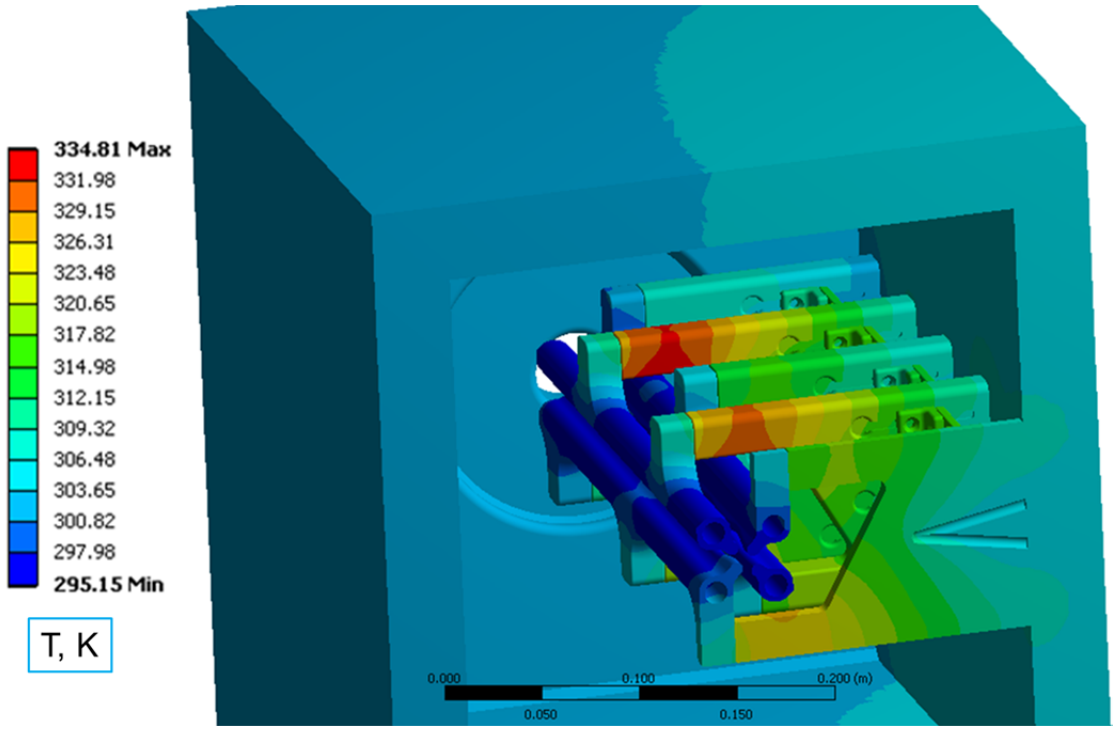

Figure 28: Temperature distribution near the end of the LANL RFQ from ANSYS thermal computations at 18% duty.

The input water velocity was taken to be 2.5 m/s and its temperature 22° C. The maximal temperature of 335 K is reached at the near-end stem, and the total temperature range is less than 40° C even in this extreme case. Maximal deformations in the RFQ structure reach 80 μm but the relative vane displacements stay below 40 μm (< 0.002″). Two important conclusions from the ANSYS thermal-stress analysis are:

(i) the proposed RFQ cooling is sufficient at all required duty factors;
(ii) additional water cooling of the tuner plates is not needed; their thermal contact with stems provides adequate cooling.

5. Summary.

We explored performance of the new 4-rod proton RFQ for the LANSCE accelerator using simulations with the CST Studio codes. Starting from a detailed engineering CAD model of the RFQ provided by Kress GmbH, the RF fields of the working mode were calculated using the CST MicroWave Studio (MWS). We found that the field quality, maximal electric field, inter-vane voltage flatness, and the frequency tuning range satisfy the requirements in the modified design with 24 stems, cf. Sec. 2.

The properly scaled RF fields were then imported in the CST Particle Studio (PS) model of the RFQ. Particle-in-cell (PIC) modeling of beam dynamics in the 4-rod LANL RFQ has been performed with PS for various initial beam currents and distributions. The combined MWS+PS simulations take into account effects associated with 3-D field asymmetries and end-gap fields, which are not predicted by standard RFQ design codes nor considered in usual beam dynamics simulations. The RFQ output beam

energy, transmission, and final beam emittances were found within the design specifications. For many cases, the PS results were checked with other beam dynamics codes, which used the MWS-calculated 3-D fields, and were confirmed. The beam dynamics results are presented in Sec. 3.

The MWS-calculated power flux was used for the RFQ thermal-stress analysis with ANSYS, cf. Sec. 4. The proposed cooling scheme was found sufficient, and the thermal-induced structure deformations are acceptable.

Our previous experience acquired in the process of CST simulations [5, 6] for the FNAL 4-rod RFQ was very valuable for evaluating the design performance of the new 4-rod LANL RFQ. Also very helpful were communications with our Fermilab and German colleagues, and feedback from the FNAL RFQ commissioning.

Acknowledgements

The author would like to thank Larry Rybarcyk, Bob Garnett, Yuri Batygin, Jim O'Hara, Eric Olivas, and Tom Wangler of LANL; Janet Schmidt and Alwin Schempp of IAP, Goethe University (Frankfurt, Germany); and Jürgen Häuser of Kress GmbH for their kind help, advices, useful information, and stimulating discussions.

6. References.

1. CST Studio Suite. CST, 2013, www.cst.com
2. R.W. Garnett et al. IPAC11 (2011), p. 2658; NA-PAC13, MOPMA14 (2013).
3. L.J. Rybarcyk et al. NA-PAC13, MOPMA17 (2013).
4. C.-Y. Tan et al. PAC11 (2011), p. 1701.
5. S.S. Kurennoy, R.W. Garnett, and L.J. Rybarcyk. IPAC13 (2013), p. 3978.
6. S.S. Kurennoy. Tech notes AOT-ABS: 2012-017 (TN); LA-UR-12-26388, Los Alamos, 2012; and AOT-HPE: 2013-005 (TN); LA-UR-13-21653, Los Alamos, 2013.
7. S.S. Kurennoy, E.R. Olivas, and L.J. Rybarcyk. NA-PAC13, MOPMA16 (2013).
8. Los Alamos Accelerator Code Group, laacg.lanl.gov
9. S.S. Kurennoy. "CST model of LANL RFQ: MicroWave Studio and Particle Studio results" Los Alamos, 5/31/13.
10. A. Schempp, Private communication, May 2013.
11. B. Koubek et al, PAC11, New York, p. 1888 (2011).
12. Y.K. Batygin. "Particle-in-cell code BEAMPATH for beam dynamics simulations in linear accelerators and beamlines." *Nucl. Instr. Meth.,* **A539**, 455 (2005).
13. Y.K. Batygin, Private communication, Oct. 2013.
14. C.-Y. Tan, Private communication, Dec. 2012.
15. ANSYS. ANSYS Inc., www.ansys.com
16. S.S. Kurennoy, S. Konecni, J. F. O'Hara, and L.J. Rybarcyk. EPAC08 (2008), p. 3431.
17. S.S. Kurennoy, L.J. Rybarcyk, J.F. O'Hara, E.R. Olivas, and T. P. Wangler. "H-mode accelerating structures with PMQ beam focusing." *Phys. Rev. ST Accel. Beams*, **15**, 090101 (2012).